Robustness of crop disease response to climate change signal under modeling uncertainties

Marie Launay, Olivier Zurfluh, Frédéric Huard, Samuel Buis, Gaétan
Bourgeois, Julie Caubel, Laurent Huber, Marie-Odile Bancal

Robustness of crop disease response to climate change signal under modeling uncertainties

Marie Launay[1], Olivier Zurfluh[2], Frederic Huard[1], Samuel Buis[3], Gaétan Bourgeois[4], Julie Caubel[5], Laurent Huber[2], Marie-Odile Bancal[2]

[1] US AgroClim, INRA, Domaine St. Paul, Site Agroparc, 84914 Avignon Cedex 9, France

[2] UMR ECOSYS, INRA, AgroParisTech, Université Paris-Saclay, 78850 Thiverval-Grignon, France

[3] UMR EMMAH, INRA, Domaine St. Paul, Site Agroparc, 84914 Avignon Cedex 9, France

[4] Agriculture and Agri-Food Canada, Horticulture Research and Development Centre, Saint-Jean-sur-Richelieu, Quebec, Canada

[5] EcoClimaSol, Immeuble MIBI, 672 Rue du Mas Verchant, 34967 Montpellier Cedex 02, France

Corresponding author:

Marie Launay

Tel: +33 4 32 72 23 67. E-mail address: marie.launay@inra.fr

Abstract

Crop fungal diseases threaten food security in the dual context of a growing global population and a warming climate. Leaf rust is one of the most important wheat diseases which can result in yield losses of more than 40%. When considering these crucial questions, innovative approaches to crop cultivation are clearly required. One essential prerequisite before the development of adaptive strategies to climate change, is to understand and forecast the potential impact of this change on fungal diseases, based on the use of modelling approaches. However, numerous epidemiological models are available; they vary considerably in terms of their complexity, and are based on hypotheses that oversimplify factors that influence the prediction of epidemics. During this study, we implemented six combinations of leaf wetness duration and infection efficiency models to simulate the future evolution of leaf rust of wheat, and compared the resulting trends. Daily and seasonal climatic indicators were inferred from the simulated infection efficiencies, from 1950 to 2100, with two contrasted Representative Concentration Pathways, RCP 4.5 and RCP 8.5, at three sites representative of traditional French wheat production areas. The inferred indicators characterize the intensity and frequency of leaf rust infection, the length and calendar positioning of the longest sequences without infection, and the relevant microclimate. Their absolute values varied considerably depending on the model combinations used, even more than between the present and future climatic periods or RCP scenarios. However, the same trends were observed in the future, with climate change being a significant explanatory variable of the evolution of the six climatic indicators simulated. The results of combining these models showed that the climatic risk of both the frequency and intensity of leaf rust infection would increase during the autumn and winter seasons, and a distinct drop should be expected during the summer, enabling a longer risk-free period. Some important common trends were thus highlighted, reinforcing confidence in the robustness of the results. These findings should be taken into account when designing adaptive strategies that will sustain production under future abiotic stresses while minimizing sanitary risks.

Highlights

1. Six combinations of models offered future trends for leaf rust of wheat

2. Climatic risk indicators assessed the intensity, frequency & duration of leaf rust

3. Future climatic conditions in the autumn and winter would favor leaf rust infection

4. A distinct drop should be expected in the summer enabling a longer risk-free period

1. Introduction

Today's challenges of food security - providing qualitative and quantitative products using sustainable agricultural systems- have as corollary the emergence of combined practices limiting both stress risk and input use. This agroecological transition in different plant production sectors is questioning research and development capacities to anticipate and propose solutions to deal with the consequences of future climatic variations on agroecosystems. From this perspective, the impacts of temperature increases and water shortage due to climate change (CC) on crops have been widely studied and many adaptation schemes to limiting abiotic factors were designed. By comparison, the impact of CC on reducing biotic factors (such as diseases, weeds and insects) remains poorly understood, particularly in the case of fungal diseases and sanitary risks (Boonekamp, 2012; Newbery et al., 2016). Nevertheless, numerous direct impacts of CC are expected on pathogens, such as an increased winter survival and a faster pathogen development due to milder winters and warmer springs, given moisture requirements are met (West et al., 2012). Thermophilic crop fungi would clearly benefit climate warming (Hulme, 2017) ; it was indeed confirmed by modelling the responses of infection or epidemics to climate drivers (Launay et al., 2014; Caubel et al., 2017), but infection risks were also found to decrease in a number of European crop pathosystems (Gouache et al., 2010; 2013; Launay et al., 2014). Properly anticipating CC impacts on crop diseases is crucial as they currently cause 16% harvest losses, and are therefore already threatening food security (Flood, 2010; Oerke, 2006; Savary et al., 2012).

In this context, models are mandatory tools to forecast CC impacts on fungal crop diseases; however they are numerous, with a large range in complexity, and rely on hypothesis that oversimplify factors influencing epidemics predictions. Models can nevertheless provide trends for the the evolution of disease risks, the robustness of which needs to be evaluated. Mostly bioclimatic models are used to predict spatial and temporal occurrence of fungal species as a function of climate (Jeschke and Strayer, 2008). Furthermore infection risk is often assumed to be the first potentially limiting step for epidemics under unlimited inoculum rates; consequently most bioclimatic models only estimate infection efficiency from wetness duration and air temperature (Magarey et al., 2005).

This simplified approach applied to leaf rust (*Puccinia triticina*), a common disease of bread wheat (*Triticum aestivum*), durum wheat (*T. turgidum var. durum*) and triticale (*X triticosecale*), for which dispersal episodes and inoculum rates impact little epidemic dynamics. Leaf rust, one of the most important wheat diseases in a wide array of climates wherever wheat is grown (Huerta-Espino et al., 2011), causes more than 40% production losses when the disease is severe on susceptible cultivars (Khan et al., 2013). Severity of this disease increased in the recent years (Morgounov et al., 2012), while climate change is expected to modify its frequency, incidence (Wojtowicz et al., 2017), severity (Junk et al., 2016) and synchronicity with host (Caubel et al., 2017). Indeed, the future increase in the frequency of extreme events such as storms should offer better conditions for wheat rust spores which are mobile and can be transported for long distances (Rosenzweig et al., 2001). Moreover, milder winters and warmer springs should favor earlier epidemics, shorten latency periods and increase infection and sporulation efficiencies, thus causing more infectious cycles (Caubel et al., 2017). However, when assessing the future impact of climate on leaf rust development, certain inconsistencies between studies can be highlighted, partly because different methods were used in the studies reviewed by Juroszek and von Tiedemann (2013). In particular, different formalisms from various models may lead to quite contrasted simulated results. In the present study, we argue that a multimodel ensemble approach, such as currently implemented in meteorology and atmospheric sciences, and already used in crop modeling (Wallach et al., 2018), might be relevant to generating robust trends for the future evolution of leaf rust of wheat.

Assuming that the infection risk remains the main gateway for wheat leaf rust epidemics in the future, we aimed to study the evolution of leaf rust infection risk with climate change, implementing various models. Three models of leaf rust infection efficiency were thus coupled with two contrasted models of dew duration, a key point in infection prediction. As infection efficiency strongly relies on wetness duration and temperature during dew period, statistical and physical modelling approaches were also -implemented to estimate wetness duration; both continuous and class modelling frames were applied to assess the resulting infection efficiency. The objectives of this paper are thus to (i) estimate the evolution of the future infection risk for wheat leaf rust and (ii) compare

the simulated tendencies according to different models of climate change, infection efficiency and leaf wetness durations. The underlying question being: is a common trend detected despite cumulated uncertainties in the modeling process?

2. Materials and methods

2.1. General description of the protocol (Fig.1)

Evolution of the climatic risk of infection regarding leaf rust of wheat was evaluated using the Representative Concentration Pathways (RCP) RCP 4.5 and RCP 8.5, associated with future CO_2 emission scenarios, from 1950 to 2100, at three sites representative of traditional French wheat production areas. Two models calculating leaf wetness duration were coupled with three models calculating the risk of infection due to leaf wetness duration and temperature. Climatic indicators of infection risk were then deduced for the purposes of the study: the number of infectious days throughout a given period, the global risk of infection throughout a period as a function of the number of infectious days and the mean infection efficiency during these days, and the length and date of the longest sequence without infection during a given period.

2.2. Climate scenarios covering the recent past and future (1950-2100)

Present and future climatic conditions (between 1950 and 2100) were performed using the ALADIN-Climat regional climate model nested within the global ARPEGE-Climat model (Déqué, 2010). Three periods were simulated: the recent past ("RP": 1976-2005), near future ("NF": 2021-2050) and far future ("FF": 2070-2099) periods, applying CO2 forcing from the IPCC emission scenario (AR5) (Moss et al., 2010). Two CO_2 RCP emission scenarios were used as developed by the IPCC (2014). We selected a pathway for the stabilization of radiative forcing by 2100, RCP 4.5, and a scenario of comparatively high greenhouse gas

emissions, RCP 8.5, projecting a rise in global mean surface temperatures from 1.5°C to 4.8°C accompanied by an average atmospheric CO_2 concentration ranging from 650 ppm to 1370 ppm by the late-21st century (Van Vuuren et al., 2011). A Quantile-Mapping approach was applied as a statistical downscaling method (Déqué, 2007) to the three selected locations in order to assess climate change, climate variability and extreme events at a regional scale. This non-parametric statistical method consists in calibrating a correction function for simulated variables as a conditional probability of observed data on the same variables (Déqué, 2007; Terray et al., 2010). Climate models usually produce an estimate of future daily temperatures, relative humidity and rainfall. Hourly values for temperature, rainfall and relative humidity were therefore generated from these daily climatic variables, following the approach described by Launay et al. (2014). With respect to air temperature, hourly assessments were obtained using a sinusoidal law with maximum and minimum temperatures taken as the temperatures at 14:00 universal time (UT) and sunrise, respectively. Daily precipitation amounts were disaggregated into hourly values using a statistical approach based on concepts proposed by Allcroft and Glasbey (2003). The method relies on a Gaussian latent process, which is transformed into a precipitation process with a power-exponential function. This transformation function provided an accurate fit for both the body and the heavy tail of the precipitation distribution, in two sites representative of the northern France climatic variability (Allard and Bourotte, 2014). Relative humidity was estimated from vapor pressure values deduced from hourly air and dew point temperatures.

2.3. Sites representative of French wheat production areas

The study was performed on three sites representative of different French climates and covering the northernmost to the southernmost wheat production areas : Estrées-Mons and Versailles correspond to the degraded oceanic climate of the North and Central plains respectively, while Bordeaux has a pure oceanic climate in the southwest part of the country (Joly et al., 2010). Furthermore, Estrées-Mons, Versailles and Bordeaux offered contrasted conditions

regarding temperature and surface wetness durations for this study. A climatic situation was considered as a combination of one site (Estrées-Mons, Versailles or Bordeaux) with one RCP scenario (4.5 or 8.5).

2.4. Models

<u>Simulating surface wetness duration</u>

Two models and modeling approaches were chosen to simulate leaf wetness duration during this study. First, the MEDHI statistical model (Launay et al., 2014) consists of a decision tree based on climatic conditions at current and previous hours, accounting for relative humidity, rain and the previous state of leaf wetness duration. It is an hourly model based on several hypotheses: (i) rainfall over 0.5 mm during the current hour leads to wetness, (ii) if no rainfall, wetness is conditioned by the relative humidity prevailing during the current hour (compared with given thresholds) and the amount of rain or wetness during the previous hour, (iii) wetness also depends on the time of day and relative humidity thresholds, and (iv) the thresholds of relative humidity are calculated by optimization to find the best values that increase overall model performance. Second, the physical Plata model is a one-layer mass and energy transfer model (Lhomme and Jimenez, 1992; Roche et al., 2008) within a family of physical models devoted to simulate condensation and evaporation of liquid water (Magarey et al., 2005; Huber & Gillespie, 1992). The variables required to simulate leaf temperature and wetness are the following: air temperature, relative humidity, wind speed, global radiation, rainfall (at a reference level above ground). Parameters of importance to estimate are the cloud cover and long-wave sky radiation, the magnitude of which is important during the nocturnal periods.

Simulating infection efficiency

Three models were selected to simulate the infection efficiency of brown rust of wheat from leaf wetness duration and air temperature during wetness periods. Firstly, two continuous relationships established by de Vallavieille-Pope et al. (1995) and Launay et al. (2014) were implemented. Both models have close formalisms, built on surface responses to the temperature and leaf wetness duration. However the model developed by de Vallavieille-Pope and colleagues (so-called "Pope model") is very flexible to parameterize, including parameters without biological meaning, and thus requires considerable experimental data to ensure its optimization. On the other hand, the ClimInfeR model is a generic model that is easier to parameterize because it relies on biological parameters such as cardinal temperatures, but has a plateau response function to temperature that causes a lack of continuity at each temperature threshold.

In the Pope model the influence of temperature during wetness periods is described using a beta function with minimal and maximal temperatures as the parameters (Eq.1). The influence of continuous leaf wetness duration on relative infection efficiency is thus calculated as the product of maximal infection and a Richards function of leaf wetness duration (Eq.2) (Fig.1.a).

$$IE_{max}(T) = p((T - T_{min})/(T_{max} - T_{min}))^n((T_{max} - T)/(T_{max} - T_{min}))^m \qquad (1)$$

With $\qquad p = (n + m)^{n+m}/(n^n m^m)$

$$IE(LWD, T) = IE_{max}(T)\left(1 - exp\left(-b(LWD - LWD_{min})\right)\right) \, for \, LWD \geq LWD_{min} \qquad (2)$$

where *T* is the air temperature during the period of leaf wetness *LWD*, *Tmin* and *Tmax* are respectively the minimum and maximum temperatures for infection (2.0 and 30.0°C respectively), *LWDmin* is the minimal dew period necessary for infection and *b* is the initial infection rate. *LWDmin* and *b* varied with temperature according to non-linear regressions (*LWDmin = 18.74 - 1.58T + 4e^{-2}T^2; b = 0.1648 - 1.3269e^{-2}T + 9.1429e^{-4}T^2*). *IE* is the relative infection efficiency, with values between 0 and 1, *LWD* is supposed to be continuous (not interrupted), and *n* and *m* are adjusted parameters (0.75 and 0.9 respectively).

In the model developed by Launay and colleagues ("ClimInfeR model") the influence of temperature during wetness periods is described using a linear-plateau function with ascending and descending portions on either side of the optimal plateau (Eq.3). Temperature influences the upper limit of the response to LWD, which is approached as the period of wetness is extended, as proposed by Duthie (1997) using a Weibull equation (Eq.4) (Fig.1.b).

$$IE_{max}(T) = \begin{cases} 0 & T \leq T_{min} \ and \ T \geq T_{max} \\ 1 & T_{opt1} \leq T \leq T_{opt2} \\ \frac{1}{(T_{opt1}-T_{min})}(T-T_{min}) & T_{min} < T < T_{opt1} \\ \frac{1}{(T_{opt2}-T_{max})}(T-T_{max}) & T_{opt2} < T < T_{max} \end{cases} \tag{3}$$

$$IE(LWD,T) = IE_{max}(T)(1 - exp\{-[A(LWD - LWD_0)]^B\}) \tag{4}$$

where *T* is the air temperature during the period of leaf wetness *LWD*, and *Tmin*, *Topt1*, *Topt2* and *Tmax* are the minimum, first optimum, second optimum and maximum temperatures for infection (1.86, 14.54, 18.36 and 31.0°C respectively). *IEmax(T)* is the maximal infection efficiency given the temperature *T*, i.e. the upper asymptote in eq.4, *A* is the intrinsic rate of increase (0.11°C), *LWD$_0$* is the length of delay before the initial response (set to nil, based on the

assumption that infection efficiency would respond immediately, although very slowly, even for a short LWD), and *B* locates the inflection point on the response axis (here the 3.12 value means that the curve infects when the response is approximately one-half the upper limit).

Finally, the simple generic infection model developed by Magarey (2005) estimates the wetness duration required to achieve a critical disease threshold at a given temperature (Eq.5&6). In the framework of this study, this model ("Magarey model") was used to determine if, given the daily wetness duration and the mean temperature during this wetness period, a day was infectious (infection efficiency higher than a 5% threshold) or not (Fig.1.c).

$$f(T) = \begin{cases} \left(\frac{T_{max}-T}{T_{max}-T_{opt}}\right)\left(\frac{T-T_{min}}{T_{opt}-T_{min}}\right)^{(T_{opt}-T_{min})/(T_{max}-T_{opt})} & T_{min} \leq T \leq T_{max} \\ 0 & T < T_{min} \ and \ T > T_{max} \end{cases} \quad (5)$$

$$LWD(T) = LWD_{min}/f(T) \leq LWD_{max} \quad (6)$$

where *T* is the air temperature during the period of leaf wetness *LWD* required to reach 5% of infection efficiency. *f(T)* is the temperature response function where *Tmin*, *Topt*, and *Tmax* are the minimum, optimum and maximum temperatures for infection (2.6, 25 and 30°C respectively). *LWDmin* is the minimum value of leaf wetness duration required to reach the 5% threshold of infection efficiency at any temperature (5 hours), and *LWDmax* is a parameter providing an upper boundary on the value of *LWD(T)* (16 hours).

All the infection model parameters for leaf rust of wheat had been adjusted previously by the authors (de Vallavieille-Pope et al. 1995 for the Pope model, Launay et al. 2014 for the ClimInfeR model and Magarey 2005 for the Magarey model).using a statistical comparison of model predictions and observations based on the published data from de Vallavieille-Pope et al. (1995).

Combinations of models

Six modeling combinations were implemented: the two wetness duration models (Medhi and Plata) were coupled to the three infection models (Pope, ClimInfeR and Magarey). Thus the infection models were fed with daily wetness durations and daily mean temperatures during wetness periods. The Pope and ClimInfeR models provided daily infection efficiencies, while the Magarey model estimated the infectious nature of each day. The six model combinations were run for RCP scenarios 4.5 and 8.5, from 1950 to 2100, concerning the three French sites at Estrées-Mons, Versailles and Bordeaux (Fig.1).

2.5. Key variables studied

In order to evaluate the impact of climate change on the evolution of leaf rust of wheat, we considered the following climatic indicators of infection risk:

- The number of infectious days throughout a period NID and NID5: a day was considered to be "infectious" when the infection efficiency simulated by the infection model (Pope, ClimInfeR or Magarey) was not null (NID) or was higher than 5% (NID5).

- The global risk of infection (GIR) throughout a period was the number of infectious days (NID as previously described) multiplied by the mean infection efficiency during these days; this integrative indicator would thus take account of both the frequency and intensity of infection throughout a period. The GIR was equivalent to a number of days of fully infection, i.e. with 100% infection efficiency.

- The length and date of the longest sequence without infection throughout a period, with LS0I being the number of successive days, and DS0I being the median date of this sequence during which infection efficiency simulated by the infection model was lower than 5%.

We then examined which climatic factor - either leaf wetness duration (LWD) or air temperature during the period of wetness T° - is best linked to future trends of leaf rust evolutions as predicted by models.

During this study, infra-annual and sliding periods were considered to calculate the indicators described above. Indeed, previous studies on the impacts of climate change on fungal crop diseases indicated the need to analyze the results at a sub-annual or even monthly scale given their intra-annual variability (Launay et al., 2014; de Vallavieille-Pope et al., 2018; Salinari et al., 2006; Skelsey et al., 2016). Moreover, in this study we did not consider host phenological stages by themselves, even though they are expected to shift with climate change (Bertin, 2008). However, we accounted for this phenomenon by calculating our climatic indicators over sliding periods, thus enabling analysis of the gap between infection peaks.

Two types of period were thus considered to calculate the climatic indicators NID5, GIR, LS0I, DS0I, LWD and T. Firstly, NID5 and GIR were calculated throughout 30-day sliding periods: these values at a given date were therefore calculated over a 30-day period around this median date. Secondly, all the climatic indicators were calculated over four seasons: their autumn value was calculated between October 15 and January 14, the winter value between January 15 and April 14, the spring value between April 15 and July 14 and the summer value between July 15 and October 14. The first three periods corresponded to the wheat crop cycle while the summer period corresponded to the fallow crop period, thus helping to highlight adaptive rules to deal with the risk of wheat rust. The NID5 seasonal value was the cumulated number of days with at least 5% infection efficiency, while the GIR seasonal value was calculated as the cumulated number of infectious days (infection efficiency not null) throughout the season, multiplied by the average infection efficiency during these days, so that it was equivalent to the cumulated number of days of full infection (100% infection efficiency). The seasonal values of LS0I and DS0I were respectively the longest number of successive days and the median date of this sequence during which infection efficiency was lower than 5%.

2.6. Statistical analysis and plots

Our objective was proposed to explain variations of the NID5, GIR, LS0I, DS0I, LWD and T climatic indicators as a function of natural spatial variations in climate, the discrepancies between the model formalisms used to calculate these climatic indicators, and climate change. We used linear models (for the LWD and T indicators) and generalized linear models (for all other climatic indicators), with the site location (Estrées-Mons, Versailles or Bordeaux), combinations of models (the Medhi and Plata leaf wetness duration models combined with the Pope, ClimInfeR and Magarey infection models) and the climatic period (recent past period "RP": 1976-2005, near future period "NF": 2021-2050 and far future period "FF": 2070-2099) as explanatory variables. Interaction terms were also included.

With respect to LWD and T, normality and homoscedasticity assumptions for the linear fitted models were verified using the D'Agostino and Bartlett tests, respectively (R package moments, Komsta and Novomestky, 2015). When significant differences were observed between climatic periods, multiple comparisons of means were performed using Tukey's honestly significant difference (HSD) procedure.

On the other hand, the NID5, GIR, LS0I and DS0I indicators were $\log_{10}$-transformed to meet normality assumptions and we assumed a Poisson error structure when fitting the associated generalized linear models. We used post hoc tests to investigate pairwise differences between climatic periods using least-squares means (the lsmeans function of lsmeans R package, Lenth 2016). All analyses were performed using the R statistical platform, version 3.5.0 (R Core Team, 2018).

To improve visualization of the impacts of the models and CC on infection efficiency, absolute or relative values for the indicators NID5 (number of infectious days with infection efficiency > 5%), GIR (infection efficiency x number of infectious days), LS0I and DS0I (length and date of the longest sequence without infection) were used. In the last case, relative values of the V variable were calculated as the V/Vmax ratio where Vmax is the maximum value of V provided

by the same combination of models over the same season, except for temperature for which the relative value was calculated as the (T-Tmin)/(Tmin-Tmax) ratio, with Tmin and Tmax being the minimum and maximum temperature values, respectively

3. Results

We first presented the mean annual variations in predicted values of NID5, GIR and LWD as well as their evolution over the year. Then we analyzed statistically their variations according to the season, using either GLM or LM in the case of NID5 and GIR, or LWD respectively. In this part, infection efficiency and LWD models were combined to evaluate whether, given the models' uncertainties cumulated, a same tendency in response to CC was found. We then focused on the date and length of periods without infection, in particular the fallow period in summer related to the future inoculum pressure. Finally, we identified the main climatic factors explaining these evolutions in seasonally trends.

3.1. Overall evolution over the year of the frequency and intensity of the climatic infection risk from 1950 to 2100

The absolute values of the NID5 and GIR climatic indicators calculated over 30-day sliding periods varied considerably depending on the model combinations used, even more than between the present and future periods or between RCP scenarios. However, the same trends could be observed in the future, whichever the models were used, and were more severe under RCP 8.5 than with the RCP 4.5 scenario.

The absolute values for climatic indicators vary considerably between different model combinations

On the annual scale, the NID5 (numbers of infectious days with an infection efficiency > 5%) mean value for all climatic situations (the three French sites and two RCP scenarios), was assessed much more lower with the Magarey model than with Pope, which in turn was also more optimistic than ClimInfeR (NID5 higher) with mean values of around 3.7 for Magarey, 11.7 for Pope and 14.1 days for ClimInfeR. Moreover, when comparing the NID5 simulations according to models of leaf wetness duration, Medhi produced lower NID5 estimates than Plata, with mean values of around 9.0 and 10.6 days for the Medhi and Plata models respectively. As for the GIR indicator (global risk of infection), differences between the simulations by different models still remained meaningful but to a lesser extent; the Magarey model was excluded because it could not calculate GIR values. The GIR annual mean values obtained showed 1.4 days of full infection more with Pope (mean around 5.5 days) than with ClimInfeR (mean around 6.9 days). As for NID5, lower GIR values were found with the Medhi model of wetness duration than with Plata (mean values of around 5.7 and 6.6 days of full infection, respectively). Finally, NID5 forecasts could be four times higher depending on the models used and their combinations, while GIR values varied by around 10% with different model combinations. More serious risks were simulated using the Pope and ClimInfeR infection models and Plata wetness duration model.

Figure 2 shows an example of the demonstrative climatic situation at the Versailles site under the RCP 8.5 scenario (other similar situations are not shown). The daily NID5 (a) or GIR (b) moving values from 1950 to 2100 (x-axis), from January 1 to December 31 (y-axis), are thus shown with figures indicated from low values (blue) to high values (red). In this specific climatic situation, NID5 values (Fig. 2a) as simulated by the Magarey model remained between 0 and 15 days most of the year (on the y-axis) throughout the 1950-2100 period (x-axis), while the NID5 values simulated by ClimInfeR often exceeded 15 days. Differences between the estimates generated by Medhi and Plata appeared to be less discriminating than between infection models. However, the Plata model produced higher estimates of leaf wetness durations (Appendix A, Table e), resulting in greater infection efficiencies than with Medhi for a given infection model. On Fig.2b, the GIR values simulated by ClimInfeR were on average higher than those simulated by the Pope model. Furthermore, GIR values

appeared to be strongly dependent of NID5 values (Fig.2a), suggesting that GIR variability is more dependent on the number of infectious days than on infection efficiency.

The same trends may be observed in the future, whichever models are used.

Whichever models were used to calculate NID5 and GIR, the trends observed were the same: future climate conditions extended the mid-year period without infection (summer), while increasing the infection frequency during autumn and winter (from December to March). Whatever the site and the RCP scenario, and as shown regarding the demonstrative situation of the Versailles site and the RCP 8.5 scenario on Fig.2a&b, the same temporal shift was observed, with hot spots of both NID5 and GIR occurring sooner in the wheat crop cycle in autumn and winter (between DOY 330 and 60 the year after) and ceasing sooner in spring, so that summer periods with little or no infection grew consistently longer in the future (around DOY 200, i.e. mid-July). The results that follow in this paper are therefore split by seasonal periods (autumn, winter, spring and summer).

3.2. Evolution of the frequency and intensity of the climatic infection risk in future seasons

The seasonal climatic indicators NID5 and GIR displayed similar trends in the future, with climate change being one of the factors significantly explaining their evolution, alongside the combination of models used to calculate them and the site (Table 1).

During the autumn and winter, NID5 and GIR could be expected to increase from the NF whatever the RCP scenario (Table 2) or site (Appendix A in Supplementary Materials, Table a). They would continue to increase in the FF, especially during the winter, under both RCP scenarios, while GIR would stagnate in the FF during the autumn under RCP scenario 4.5 (Table 2 and Appendix A, Table b). From mid-October to mid-April (autumn and winter periods as defined

above) the total number of days with more than 5% of infection efficiency NID5 may increase by about 9 to 20 days between the recent past and far future, depending on the site (Appendix A, Table a). At the same time, and during the same calendar period, the total equivalent number of days with full infection GIR should increase from 9 to 16 days, revealing that an increase in both the frequency and intensity of leaf rust infection during the first part of the wheat crop cycle could be feared in the future because of climate change.

During the spring, NID5 and GIR could be expected to increase in the near future under both RCP scenarios, and then decrease in the far future (Table 2), leading to a situation similar to that in the recent past under RCP scenario 4.5, and to a less risky climatic situation in the far future under RCP scenario 8.5 (with 2 to 6 fewer infectious days, Appendix A, Tables a and b).

During the summer, the NID5 and GIR should decrease in the far future whatever the site and RCP scenario, and even in the near future under RCP scenario 8.5 (Table 2). During the fallow crop period, between mid-July and mid-October, the cumulated period favorable to infection (NID5) could thus decrease by about one month under the most pessimistic scenario, RCP 8.5.

Finally, the climatic risk of infection would not evolve in the same way at different sites: in the south (Bordeaux), the number of NID5 infectious days in the autumn and winter would increase less than in the northern part of the country (Versailles, and even more Estrées-Mons), while during the summer the number of days equivalent to GIR full infection would decrease to a greater extent (Appendix A, Tables a and b).

To illustrate these general trends, the mean seasonal values for the NID5 and GIR indicators over the four seasons in the near and far future were compared to the recent past (Fig.3) at the intermediate site in Versailles and under the most meaningful scenario RCP 8.5.

3.3. Evolution of the length and date of periods without infection

The length of autumn and winter periods without infection LS0I could be expected to decrease significantly, both in the near future in autumn under both RCP scenarios, as in winter for the RCP scenario 8.5 only (Table 2). The longest sequences of successive days without infection would thus be shortened by about 1 to 9 days during the first part of the wheat crop cycle, depending on the site and RCP scenario. The length of spring periods without infection would only increase under scenario RCP8.5 in the far future. However, summer periods without infection would significantly increase by between 6 and 12 days, in the near future, whatever the site and scenario (Appendix A, Table c).

The median DS0I dates of winter periods without infection would be advanced in the near future and postponed in the far future, while spring periods without infection should be postponed in the far future, under both RCP scenarios (Table 2). In the far future, this delay would reach one week in winter and two weeks in spring under scenario RCP 8.5 (Appendix A, Table d). No general and significant trend could be highlighted regarding the autumn and summer periods, while marked heterogeneity might be observed between sites and RCP scenarios.

To illustrate these general trends, the mean seasonal values for the LS0I and DS0I indicators over the four seasons in the near and far future were compared with the recent past (Fig.4) at the intermediate site in Versailles and under the most meaningful scenario, RCP 8.5.

3.4. Evolutions affecting temperature and wetness duration may explain all these simulated trends

Temperatures during wetness periods are expected to increase significantly (Table 3) from the near future whatever the season and RCP scenario, and to stagnate in autumn in the far future under scenario RCP 4.5, while they should continue to increase during other seasons under both scenarios (Table 4). Leaf

wetness duration should decrease significantly (Table 3) in the far future in all seasons according to scenario RCP 8.5, and only in autumn and summer under scenario RCP 4.5. Warming in the autumn and winter would be the main driver of higher values for GIR indicators, as shown in Fig.5a and Fig.5b, which shows GIR evolutions from the recent past to the far future versus changes to mean temperatures during wetness periods, over different sites and RCP scenarios. This also explains the reduction in the length of LS0I periods without infection, particularly in winter (Fig.5c). Conversely, shorter leaf wetness durations in THE spring and summer would explain both the lower GIR values (Fig.5d and Fig.5e) and shorter periods without infection (Fig. 5f).

4. Discussion

During this study, our aim was to estimate changes to the climatic risk of infection with respect to leaf rust of wheat using different model combinations and modelling approaches. Our hypothesis was that despite the different models implemented, the impacts of climate change on wheat disease would be similar. Our findings revealed that the absolute values of the simulated climatic indicators varied considerably depending on the model combinations employed, even more than between present and future periods or RCP scenarios. However, the same trends were observed for the future, with climate change being a significant explanatory variable for evolutions of the six climatic indicators we simulated. These indicators characterized the intensity and frequency of leaf rust infection, the length and calendar positioning of the longest sequences without infection, and the leaf wetness duration and air temperature during wetness periods. This multimodel ensemble approach is common in the literature on meteorology and atmospheric sciences, and has already been used in crop modelling, particularly to compare crop model performance when assessing yield under various abiotic stresses (Wallach et al., 2018). But to our knowledge this is the first time that this approach has been implemented with respect to crop health. Although only a few models were involved in this study, they were markedly different and based on statistical or physical formalisms, continuous or threshold response functions. This partly explains the broad range

of simulated values obtained for the six climatic indicators. In our case it was therefore not relevant to use the mean value of simulations from different model combinations as a predictor (Martre et al., 2015). However, this combined approach did produce some homogeneous trends regarding the future evolution of leaf rust of wheat, thus reinforcing confidence in the robustness of these results.

We were able to show that both the frequency and intensity of leaf rust infection would increase in France during the first part of the wheat crop cycle, whatever the RCP scenario. The number of infectious days between mid-October and mid-April would therefore increase by almost 1 to 3 weeks, depending on the site and RCP scenario. By contrast, the climatic risk of infection should stagnate or diminish in the far future during the spring and summer periods, while a temporary rise in the frequency of infection might occur in the spring in the near future. During the fallow period between mid-July and mid-October, the reduction in the cumulated period favorable to infection could reach up to one month. Moreover, evolutions in the southern part of France would differ from those in the north, with the frequency and intensity of infection increasing to a lesser extent in autumn and winter, and decreasing to a greater extent in the summer. This could be related to the warmer climate in southern France, with autumn and winter temperatures already closer to the optimum infection temperature than in the north, and summer temperatures reaching the maximum temperature for infection in the far future.

These findings confirm and reinforce previous findings which forecast a greater and earlier climatic risk of infection during the winter (Junk et al., 2016; Launay et al., 2017). Moreover, we analyzed the seasonality of the disease risk, and were thus able to reveal contrasted trends during the year, with a significant and general increase in the climatic risk during the cold (but milder) autumn and winter seasons, and a distinct drop during summer. Both tendencies could be explained by warmer autumns and winters and dryer summers. In addition, we also considered periods without an infection risk in terms of their length and date. As the length of the longest sequences of days without infection obviously evolved contrary to the frequency of infection risk, the date of such "safe"

periods was shown to be delayed until the end of spring, shifting from mid-May to early-June. When implementing the six combinations of leaf wetness duration and infection efficiency models, we noted marked differences between surface response models on the one hand (Pope and ClimInfeR) and the Magarey threshold model on the other. This could be explained by the infection values of less than 5% simulated by the Magarey model for temperatures below 16°C and leaf wetness durations shorter than 16 hours (Fig.1), while both the Pope and ClimInfeR models simulated higher infection efficiencies for the same range of temperatures and wetness durations. A significant number of days were thus considered to be non-infectious by the Magarey model, as shown in Fig. 6. Even if the same experimental data were used to calibrate the three models (de Vallavieille-Pope et al., 1995), the predicted risk of infection differed between the models for a wide (and common) range of temperatures and wetness durations. As previously noted for yellow rust of wheat, *Puccinia striiformis* f.sp. *tritici* (de Vallavieille-Pope et al., 2018), the parameterization of response functions relative to infection efficiencies could be improved for low (or even moderate) temperatures, thanks to additional experimental data.

Certain areas of uncertainty still need to be investigated. Rainfall forecast are crucial when estimating leaf wetness duration, but they remain very unreliable and climate models may produce markedly different predictions. In the summer, the ALADIN-Climat regional climate model we used predicted an average reduction of 0.38 mm.day^{-1} in France between [1976-2005] and [2071-2100] under the RCP 8.5 scenario while the WRF (Weather Research and Forecasting) model proposed by the US National Center for Atmospheric Research predicted an overall increase of the same scope (+0.32mm.day^{-1}) (Jouzel et al., 2014). However, the two regional climate models Aladin-Climat and WRF agreed on a slight increase in average precipitation in summer and winter by 2050, and an increase in winter precipitation by the end of the century. The two models thus simulated small changes in the percentages of extreme precipitation, and these results were within the low range of the European multi-model set (Jouzel et al., 2014).

Recent studies have demonstrated the adaptive response of pathogens to temperature achieved by their intra-specific diversity (de Vallavieille-Pope et al., 2018; Mariette et al., 2016). This acclimation of pathogens to temperature, especially for those with a broad geographical distribution and re-emerging worldwide, suggests that we must take account of these patterns of local adaptation to climate in order to update the parameterization of our infection models. In this way, the invasive capacity and epidemic potential of leaf rust of wheat would be better explained and predicted in the future.

Finally, if the seasonality of the infection risk shifts, host phenology may also move because of a warming climate, causing changes to host-pathogen synchronism (Caubel et al., 2017). At the same time, crop adaptation strategies to climate change (mainly concerning abiotic stresses alone) will result in new agricultural patterns, challenging our ability to identify the levers for adaptation that will sustain production under future abiotic stresses while minimizing sanitary risks (Juroszek and von Teidemann, 2015; Hulme, 2017). In this context, it will be necessary to adopt a systemic approach that takes account of both the direct and indirect impacts of climate change (through host phenology and cropping system adaptations) on the evolution of crop disease. The methodology we developed during this study could constitute such a tool, providing useful information for stakeholders looking for warning signals and agronomic levers to manage crop health. For instance, in the case of our leaf rust of wheat pathosystem, the indicators simulated suggested that survival of the pathogen might be endangered during the fallow period. To take advantage of this climatic opportunity, farmers could grow crops such as legumes that compete with grass weeds and cereal volunteers, and could potentially provide other ecological services (Vrignon-Bregnas et al., 2018). Similarly, more favorable conditions for infection in the autumn and winter were demonstrated with a certain degree of confidence, thanks to the implementation of several models. Account could be taken of these findings when considering sowing dates in the context of adaptation strategies so as to avoid later heat and drought stress during the grain filling stage. Our climatic indicators of infection risk completed with climatic indicators relying on other epidemic phases such as survival or latency, would therefore be relevant in multicriteria analyses to evaluate the performance of adaptive strategies (Ravier et al., 2015).

5. Conclusion

By implementing six combinations of models, our study was able to offer general trends for the future evolution of the risk of leaf rust infection in the context of climate change. Despite the differences between the absolute infection risk values thus simulated, some important common trends were highlighted, thus reinforcing confidence in the robustness of the results: the climatic risk regarding both the frequency and intensity of leaf rust infection would increase in France during the autumn and winter seasons, and a distinct drop should be expected during the summer, enabling a longer risk-free period. Survival of the pathogen could thus be endangered during the fallow period, while more favorable conditions for infection in the autumn and winter will need to be addressed. The methodology we developed during this study, and the results we obtained on leaf rust of wheat, offer new opportunities for farmers and stakeholders to identify levers for adaptation that will sustain production under future abiotic stresses while minimizing sanitary risks.

References :

Allard, D., Bourotte, M., 2015. Disaggregating daily precipitations into hourly values with a transformed censored latent Gaussian process. Stochastic Environmental Research and Risk Assessment 29, 453-462.

Allcroft, D.J., Glasbey, C.A., 2003. A latent Gaussian Markov random-field model for spatio-temporal rainfall disaggregation. J. R. Stat. Soc. Ser. C (Appl. Stat.) 52, 487–498.

Bertin, R.I., 2008. Plant phenology and distribution in relation to recent climate change. J. Torrey Bot. Soc. 135, 126-146.

Boonekamp, P., 2012. Are plant diseases too much ignored in the climate change debate? European Journal of Plant Pathology 133, 291-294.

Caubel, J., Launay, M., Ripoche, D., Gouache, D., Buis, S., Huard, F., Huber, L., Brun, F., Bancal, M.O., 2017. Climate change effects on leaf rust of wheat: Implementing a coupled crop-disease model in a French regional application. Eur. J. Agron. 90, 53-66.

de Vallavieille-Pope, C., Bahri, B., Leconte, M., Zurfluh, O., Belaid, Y., Maghrebi, E., Huard, F., Huber, L., Launay, M., Bancal, M.O., 2018. Thermal generalist behaviour of invasive Puccinia striiformis f. sp tritici strains under current and future climate conditions. Plant Pathol. 67, 1307-1320.

de Vallavieille-Pope, C., Huber, L., Leconte, M., Goyeau, H., 1995. Comparative effects of temperature and interrupted wet periods on germination, penetration, and infection of *puccinia-recondita* f. sp. *tritici* and *p-striiformis* on wheat seedlings. Phytopathology 85, 409-415.

Déqué, M., 2007. Frequency of precipitation and temperature extremes over France in an anthropogenic scenario: Model results and statistical correction according to observed values. Glob. Planet. Change 57, 16-26.

Déqué, M., 2010. Regional climate simulation with a mosaic of RCMs. Meteorologische Zeitschrift 19, 259-266.

Duthie, J.A., 1997. Models of the response of foliar parasites to the combined effects of temperature and duration of wetness. Phytopathology 87, 1088-1095.

Flood, J., 2010. The importance of plant health to food security. Food Security 2, 215-231.

Gouache, D., Bensadoun, A., Brun, F., Page, C., Makowski, D., Wallach, D., 2013. Modelling climate change impact on Septoria tritici blotch (STB) in France: Accounting for climate model and disease model uncertainty. Agric. For. Meteorol. 170, 242-252.

Gouache, D., Roche, R., Pieri, P., Bancal, M.-O., 2010. Evolution of some pathosystems on wheat and vines. In: Brisson, N., Levrault, F. (Eds.), Climate change, Agriculture and forests in france: simulations of the impacts on the main species. The Green Book of the CLIMATOR project (2007-2010), part C (The crops), section B5 Health, pp. 113-126.

Huber, L., Gillespie, T.J., 1992. Modeling leaf wetness in relation to plant-disease epidemiology. Annu. Rev. Phytopathol. 30, 553-577.

Huerta-Espino, J., Singh, R.P., German, S., McCallum, B.D., Park, R.F., Chen, W.Q., Bhardwaj, S.C., Goyeau, H., 2011. Global status of wheat leaf rust caused by Puccinia triticina. Euphytica 179, 143-160.

Hulme, P.E., 2017. Climate change and biological invasions: evidence, expectations, and response options. Biological Reviews 92, 1297-1313.

Jeschke, J.M., Strayer, D.L., 2008. Usefulness of bioclimatic models for studying climate change and invasive species. Year in Ecology and Conservation Biology 2008 1134, 1-24.

Joly, D., Brossard, T., Cardot, H., Cavailhes, J., Hilal, M., Wavresky, P., 2010. Les types de climats en France, une construction spatiale. Cybergeo : European Journal of Geography; URL : http://cybergeo.revues.org/23155 ; DOI : 10.4000/cybergeo.23155.

Jouzel, J., Ouzeau, G., Déqué, M., Jouini, M., Planton, S., Vautard, R., 2014. Le climat de la France au XXIe siècle Volume 4 Scénarios régionalisés: édition 2014 pour la métropole et les régions d'outre-mer. Rapports de la Direction générale de l'Énergie et du Climat, Ministère de l'Ecologie, du Développement durable et de l'Energie, 64 p.

Junk, J., Kouadio, L., Delfosse, P., El Jarroudi, M., 2016. Effects of regional climate change on brown rust disease in winter wheat. Clim. Change 135, 439-451.

Juroszek, P., von Tiedemann, A., 2013. Climate change and potential future risks through wheat diseases: a review. European Journal of Plant Pathology 136, 21-33.

Juroszek, P., von Tiedemann, A., 2015. Linking plant disease models to climate change scenarios to project future risks of crop diseases: a review. Journal of Plant Diseases and Protection 122, 3-15.

Khan, M.H., Bukhari, A., Dar, Z.A., Rizvi, S.M., 2013. Status and strategies in breeding for rust resistance in wheat. Agricultural Sciences Vol.04No.06, 10.

Komsta, L., Novomestky, F., 2015. moments: Moments, cumulants, skewness, kurtosis and related tests. R package version 0.14. https://CRAN.R-project.org/package=moments.

Launay, M., Caubel, J., Bourgeois, G., Huard, F., de Cortazar-Atauri, I.G., Bancal, M.O., Brisson, N., 2014. Climatic indicators for crop infection risk: Application to climate change impacts on five major foliar fungal diseases in Northern France. Agric. Ecosyst. Environ. 197, 147-158.

Lenth, R.V., 2016. Least-Squares Means: The R Package lsmeans. Journal of Statistical Software 69, 1-33.

Lhomme, J.P., Jimenez, F., 1992. Estimating dew duration on banana and plantain leaves from standard meteorological observations. Agric. For. Meteorol. 62, 263-274.

Magarey, R.D., Sutton, T.B., Thayer, C.L., 2005. A simple generic infection model for foliar fungal plant pathogens. Phytopathology 95, 92-100.

Mariette, N., Androdias, A., Mabon, R., Corbiere, R., Marquer, B., Montarry, J., Andrivon, D., 2016. Local adaptation to temperature in populations and clonal lineages of the Irish potato famine pathogen Phytophthora infestans. Ecology and Evolution 6, 6320-6331.

Martre, P., Wallach, D., Asseng, S., Ewert, F., Jones, J.W., Rotter, R.P., Boote, K.J., Ruane, A.C., Thorburn, P.J., Cammarano, D., Hatfield, J.L., Rosenzweig, C., Aggarwal, P.K., Angulo, C., Basso, B., Bertuzzi, P., Biernath, C., Brisson, N., Challinor, A.J., Doltra, J., Gayler, S., Goldberg, R., Grant, R.F., Heng, L., Hooker, J., Hunt, L.A., Ingwersen, J., Izaurralde, R.C., Kersebaum, K.C., Muller, C., Kumar, S.N., Nendel, C., O'Leary, G., Olesen, J.E., Osborne, T.M., Palosuo, T., Priesack, E., Ripoche, D., Semenov, M.A., Shcherbak, I., Steduto, P., Stockle, C.O., Stratonovitch, P., Streck, T., Supit, I., Tao, F.L., Travasso, M., Waha, K., White, J.W., Wolf, J., 2015. Multimodel ensembles of wheat growth: many models are better than one. Glob. Change Biol. 21, 911-925.

Morgounov, A., Tufan, H.A., Sharma, R., Akin, B., Bagci, A., Braun, H.J., Kaya, Y., Keser, M., Payne, T.S., Sonder, K., McIntosh, R., 2012. Global incidence of wheat rusts and powdery mildew during 1969-2010 and durability of resistance of winter wheat variety Bezostaya 1. European Journal of Plant Pathology 132, 323-340.

Moss, R.H., Edmonds, J.A., Hibbard, K.A., Manning, M.R., Rose, S.K., van Vuuren, D.P., Carter, T.R., Emori, S., Kainuma, M., Kram, T., Meehl, G.A., Mitchell, J.F.B., Nakicenovic, N., Riahi, K., Smith, S.J., Stouffer, R.J., Thomson, A.M., Weyant, J.P., Wilbanks, T.J., 2010. The next generation of scenarios for climate change research and assessment. Nature 463, 747-756.

Newbery, F., Qi, A.M., Fitt, B.D.L., 2016. Modelling impacts of climate change on arable crop diseases: progress, challenges and applications. Current Opinion in Plant Biology 32, 101-109.

Oerke, E.C., 2006. Crop losses to pests. Journal of Agricultural Science 144, 31-43.

R Core Team, 2018. R: A Language and Environment for Statistical Computing.

Ravier, C., Prost, L., Jeuffroy, M.H., Wezel, A., Paravano, L., Reau, R., 2015. Multi-criteria and multi-stakeholder assessment of cropping systems for a result-oriented water quality preservation action programme. Land Use Policy 42, 131-140.

Roche, R., Bancal, M.O., Gagnaire, N., Huber, L., 2008. Potential impact of climate change on brown wheat rust: a preliminary study based on biophysical modelling of infection events and plant-pathogen interactions. Aspects of Applied Biology, 135-142.

Rosenzweig, C., Iglesias, A., Yang, X.B., Epstein, P.R., Chivian, E., 2001. Climate Change and Extreme Weather Events; Implications for Food Production, Plant Diseases, and Pests. Global Change & Human Health 2, 90-104.

Salinari, F., Giosue, S., Tubiello, F.N., Rettori, A., Rossi, V., Spanna, F., Rosenzweig, C., Gullino, M.L., 2006. Downy mildew (Plasmopara viticola) epidemics on grapevine under climate change. Glob. Change Biol. 12, 1299-1307.

Savary, S., Nelson, A., Willocquet, L., Pangga, I., Aunario, J., 2012. Modeling and mapping potential epidemics of rice diseases globally. Crop Prot. 34, 6-17.

Skelsey, P., Cooke, D.E.L., Lynott, J.S., Lees, A.K., 2016. Crop connectivity under climate change: future environmental and geographic risks of potato late blight in Scotland. Glob. Change Biol. 22, 3724-3738.

Terray, L., Page, C., Deque, C., Flecher, C., 2010. Climate change in France from several agroclimate indicators. In: Brisson, N., Levrault, F. (Ed.), The Green Book of the CLIMATOR Project. ADEME, pp. 19-32.

van Vuuren, D.P., Edmonds, J., Kainuma, M., Riahi, K., Thomson, A., Hibbard, K., Hurtt, G.C., Kram, T., Krey, V., Lamarque, J.-F., Masui, T., Meinshausen, M., Nakicenovic, N., Smith, S.J., Rose, S.K., 2011. The representative concentration pathways: an overview. Clim. Change 109, 5.

Vrignon-Brenas, S., Celette, F., Piquet-Pissaloux, A., Corre-Hellou, G., David, C., 2018. Intercropping strategies of white clover with organic wheat to improve the trade-off between wheat yield, protein content and the provision of ecological services by white clover. Field Crop. Res. 224, 160-169.

Wallach, D., Martre, P., Liu, B., Asseng, S., Ewert, F., Thorburn, P.J., Ittersum, M., Aggarwal, P.K., Ahmed, M., Basso, B., Biernath, C., Cammarano, D., Challinor, A.J., Sanctis, G., Dumont, B., Rezaei, E.E., Fereres, E., Fitzgerald, G.J., Gao, Y., Garcia-Vila, M., Gayler, S., Girousse, C., Hoogenboom, G., Horan, H., Izaurralde, R.C., Jones, C.D., Kassie, B.T., Kersebaum, K.C., Klein, C., Koehler, A.K., Maiorano, A., Minoli, S., Mueller, C., Kumar, S.N., Nendel, C., O'Leary, G.J., Palosuo, T., Priesack, E., Ripoche, D., Roetter, R.P., Semenov, M.A., Stockle, C., Stratonovitch, P., Streck, T., Supit, I., Tao, F., Wolf, J., Zhang, Z., 2018. Multimodel ensembles improve predictions of crop-environment-management interactions. Glob. Change Biol. 24, 5072-5083.

West, J.S., Townsend, J.A., Stevens, M., Fitt, B.D.L., 2012. Comparative biology of different plant pathogens to estimate effects of climate change on crop diseases in Europe. European Journal of Plant Pathology 133, 315-331.

Wojtowicz, A., Wojtowicz, M., Sigvald, R., Pasternak, M., 2017. Predicting the effects of climate change on the latency period of wheat leaf rust in western Poland. Acta Agric. Scand. Sect. B-Soil Plant Sci. 67, 223-234.

Table 1. Type II results of analyses of climatic indicators of leaf rust of wheat: generalized linear models to test the effect of natural spatial variations in the climate ("Site" effect), discrepancies between the model formalisms used to calculate the climatic indicators ("Models" effect), and the climatic period ("Climate change" effect), under the future scenarios RCP 4.5 and 8.5. Significant effects are shown in bold. Details of the effects of different climatic periods are shown in Table 2.

| | Autumn | | | | | | Winter | | | | | | Spring | | | | | | Summer | | | | | |
| | RCP 4.5 | | | RCP 8.5 | | | RCP 4.5 | | | RCP 8.5 | | | RCP 4.5 | | | RCP 8.5 | | | RCP 4.5 | | | RCP 8.5 | | |
	χ^2	df	Pr(>χ2)	χ^2	df	Pr(>χ2)	χ^2	df	Pr(>χ2)	χ^2	df	Pr(>χ2)	χ^2	df	Pr(>χ2)	χ^2	df	Pr(>χ2)	χ^2	df	Pr(>χ2)	χ^2	df	Pr(>χ2)
NID5																								
Models	7227.6	5	**<0.0001**	8277.2	5	**<0.0001**	10627.6	5	**<0.0001**	11345.4	5	**<0.0001**	22354.5	5	**<0.0001**	20687.7	5	**<0.0001**	13109.2	5	**<0.0001**	11047.8	5	**<0.0001**
Climate change (CC)	342.8	2	**<0.0001**	337.1	2	**<0.0001**	732.4	2	**<0.0001**	828.3	2	**<0.0001**	34.7	2	**<0.0001**	413.8	2	**<0.0001**	588.6	2	**<0.0001**	1772.7	2	**<0.0001**
Site	414.2	2	**<0.0001**	273.4	2	**<0.0001**	1640.5	2	**<0.0001**	1387.4	2	**<0.0001**	475.8	2	**<0.0001**	511.0	2	**<0.0001**	366.1	2	**<0.0001**	493.1	2	**<0.0001**
Models x CC	29.7	10	**0.0010**	124.0	10	**<0.0001**	32.2	10	**0.0004**	57.6	10	**<0.0001**	40.1	10	**<0.0001**	99.3	10	**<0.0001**	35.1	10	**0.0001**	191.4	10	**<0.0001**
Models x Site	34.9	10	**0.0001**	32.6	10	**0.0003**	65.0	10	**<0.0001**	59.9	10	**<0.0001**	60.7	10	**<0.0001**	104.7	10	**<0.0001**	218.9	10	**<0.0001**	274.5	10	**<0.0001**
CC x Site	32.3	4	**<0.0001**	102.7	4	**<0.0001**	91.5	4	**<0.0001**	88.1	4	**<0.0001**	21.0	4	**<0.0001**	62.4	4	**<0.0001**	14.8	4	**<0.0001**	54.4	4	**<0.0001**
Models x CC x Site	2.0	20	1	3.0	20	1.0000	7.9	20	0.9925	11.6	20	0.9299	14.0	20	0.8291	17.4	20	0.6275	12.0	20	0.9170	25.8	20	0.1729
GIR																								
Models	475.8	3	**<0.0001**	532.8	3	**<0.0001**	879.1	3	**<0.0001**	954.8	3	**<0.0001**	286.5	3	**<0.0001**	250.5	3	**<0.0001**	129.9	3	**<0.0001**	116.2	3	**<0.0001**
Climate change (CC)	333.2	2	**<0.0001**	752.4	2	**<0.0001**	366.1	2	**<0.0001**	562.4	2	**<0.0001**	25.5	2	**<0.0001**	321.7	2	**<0.0001**	228.7	2	**<0.0001**	828.3	2	**<0.0001**
Site	581.5	2	**<0.0001**	440.0	2	**<0.0001**	979.0	2	**<0.0001**	902.0	2	**<0.0001**	337.4	2	**<0.0001**	346.2	2	**<0.0001**	220.3	2	**<0.0001**	245.8	2	**<0.0001**
Models x CC	1.8	6	0.9356	1.2	6	0.9788	2.7	6	0.8425	7.0	6	0.3245	9.4	6	0.1514	16.5	6	0.0111	4.8	6	0.5691	15.9	6	0.0144
Models x Site	3.2	6	0.7829	3.5	6	0.7381	28.2	6	**<0.0001**	31.9	6	**<0.0001**	21.3	6	**0.0016**	27.4	6	**0.0001**	21.9	6	**0.0013**	21.8	6	**0.0013**
CC x Site	10.1	4	0.0384	46.0	4	**<0.0001**	17.5	4	0.0016	17.8	4	0.0014	19.9	4	**0.0005**	30.7	4	**<0.0001**	10.8	4	0.0293	24.6	4	**<0.0001**
Models x CC x Site	0.2	12	1.0000	0.6	12	1.0000	0.7	12	1.0000	0.8	12	1.0000	1.8	12	0.9997	2.1	12	0.9992	0.6	12	1.0000	0.9	12	1.0000
LSOI																								
Models	1400.3	5	**<0.0001**	1567.1	5	**<0.0001**	6128.6	5	**<0.0001**	6596.2	5	**<0.0001**	14816.0	5	**<0.0001**	13343.2	5	**<0.0001**	6708.9	5	**<0.0001**	6039.3	5	**<0.0001**
Climate change (CC)	243.9	2	**<0.0001**	188.6	2	**<0.0001**	392.3	2	**<0.0001**	196.2	2	**<0.0001**	2.3	2	**<0.0001**	95.5	2	**<0.0001**	555.4	2	**<0.0001**	916.0	2	**<0.0001**
Site	210.0	2	**<0.0001**	123.9	2	**<0.0001**	710.6	2	**<0.0001**	446.8	2	**<0.0001**	70.6	2	**<0.0001**	57.5	2	**<0.0001**	362.9	2	**<0.0001**	310.7	2	**<0.0001**
Models x CC	12.8	10	0.2374	78.9	10	**<0.0001**	181.0	10	**<0.0001**	277.0	10	**<0.0001**	21.4	10	0.0188	167.3	10	**<0.0001**	256.1	10	**<0.0001**	572.6	10	**<0.0001**
Models x Site	38.3	10	**<0.0001**	67.1	10	**<0.0001**	228.2	10	**<0.0001**	169.3	10	**<0.0001**	148.9	10	**<0.0001**	141.6	10	**<0.0001**	154.9	10	**<0.0001**	300.9	10	**<0.0001**
CC x Site	60.1	4	**<0.0001**	85.7	4	**<0.0001**	20.6	4	**0.0004**	132.4	4	**<0.0001**	30.8	4	**<0.0001**	7.2	4	0.1252	20.7	4	**0.0004**	28.3	4	**<0.0001**
Models x CC x Site	9.8	20	0.9715	9.6	20	0.9743	22.7	20	0.3040	51.2	20	**0.0002**	56.6	20	**<0.0001**	87.4	20	**<0.0001**	49.1	20	**0.0003**	79.8	20	**<0.0001**
DSOI																								
Models	7851.3	5	**<0.0001**	9716.7	5	**<0.0001**	952.5	5	**<0.0001**	905.0	5	**<0.0001**	100.4	5	**<0.0001**	140.7	5	**<0.0001**	13.9	5	0.0161	16.1	5	**0.0065**
Climate change (CC)	4.2	2	0.1235	18.0	2	**0.0001**	297.7	2	**<0.0001**	277.7	2	**<0.0001**	123.0	2	**<0.0001**	698.1	2	**<0.0001**	8.2	2	0.0162	5.8	2	0.0537
Site	19.0	2	**<0.0001**	135.1	2	**<0.0001**	74.7	2	**<0.0001**	94.7	2	**<0.0001**	24.6	2	**<0.0001**	8.4	2	0.0153	11.5	2	**0.0032**	10.4	2	**0.0054**
Models x CC	104.7	10	**<0.0001**	335.8	10	**<0.0001**	62.2	10	**<0.0001**	107.1	10	**<0.0001**	147.7	10	**<0.0001**	303.5	10	**<0.0001**	11.1	10	0.3508	9.9	10	0.4497
Models x Site	74.2	10	**<0.0001**	512.9	10	**<0.0001**	31.4	10	**0.0005**	65.1	10	**<0.0001**	18.5	10	0.0473	21.5	10	0.0179	2.5	10	0.9902	13.5	10	0.1982
CC x Site	104.2	4	**<0.0001**	43.7	4	**<0.0001**	9.1	4	0.0584	24.3	4	**<0.0001**	15.0	4	**0.0047**	22.6	4	**0.0002**	7.8	4	0.0975	21.4	4	**0.0003**
Models x CC x Site	343.6	20	**<0.0001**	284.6	20	**<0.0001**	83.1	20	**<0.0001**	69.1	20	**<0.0001**	61.1	20	**<0.0001**	53.9	20	**<0.0001**	8.4	20	0.9893	9.8	20	0.9721

Notes: Climatic indicators are defined as follows: NID5 is the cumulated number of infectious days (infection efficiency higher than 5%) throughout autumn, winter, spring or summer; GIR is the average global risk of infection calculated as the number of infectious days (NID5) multiplied by the mean infection efficiency during these days; LS0I is the cumulated number of successive days, and DS0I is the median date of this sequence during which the infection efficiency simulated by the infection model is lower than 5%.

Table 2. Pairwise comparison of the seasonal effects of climatic periods (recent past period "RP": 1976-2005; near future period "NF": 2021-2050 and far future period "FF": 2070-2099) on climatic indicators for leaf rust of wheat under scenarios RCP 4.5 and 8.5.

| Climatic periods			RCP 4.5					RCP 8.5				
			Estimate	SE	df	T ratio	P	Estimate	SE	df	T ratio	P
NID5												
Autumn	RP *vs.* NF		-0.19	0.01	Inf	-17.59	**<0.0001**	-0.12	0.01	Inf	-11.26	**<0.0001**
	RP *vs.* FF		-0.11	0.01	Inf	-10.37	**<0.0001**	-0.15	0.01	Inf	-13.30	**<0.0001**
	NF *vs.* FF		0.08	0.01	Inf	7.16	**<0.0001**	-0.02	0.01	Inf	-2.13	0.0843
Winter	RP *vs.* NF		-0.13	0.02	Inf	-7.30	**<0.0001**	-0.15	0.02	Inf	-8.77	**<0.0001**
	RP *vs.* FF		-0.34	0.02	Inf	-20.43	**<0.0001**	-0.34	0.02	Inf	-20.72	**<0.0001**
	NF *vs.* FF		-0.21	0.02	Inf	-13.01	**<0.0001**	-0.19	0.02	Inf	-11.88	**<0.0001**
Spring	RP *vs.* NF		-0.09	0.02	Inf	-5.71	**<0.0001**	-0.13	0.02	Inf	-8.61	**<0.0001**
	RP *vs.* FF		-0.03	0.02	Inf	-1.60	0.2448	0.05	0.02	Inf	2.88	0.0110
	NF *vs.* FF		0.06	0.02	Inf	4.21	**<0.0001**	0.18	0.02	Inf	11.94	**<0.0001**
Summer	RP *vs.* NF		0.02	0.01	Inf	1.65	0.2230	0.08	0.01	Inf	5.61	**<0.0001**
	RP *vs.* FF		0.23	0.02	Inf	15.22	**<0.0001**	0.43	0.02	Inf	27.18	**<0.0001**
	NF *vs.* FF		0.21	0.02	Inf	13.62	**<0.0001**	0.34	0.02	Inf	21.59	**<0.0001**
GIR												
Autumn	RP *vs.* NF		-0.30	0.02	Inf	-16.89	**<0.0001**	-0.24	0.02	Inf	-13.81	**<0.0001**
	RP *vs.* FF		-0.26	0.02	Inf	-14.65	**<0.0001**	-0.46	0.02	Inf	-27.40	**<0.0001**
	NF *vs.* FF		0.04	0.02	Inf	2.28	0.0583	-0.22	0.02	Inf	-13.92	**<0.0001**
Winter	RP *vs.* NF		-0.22	0.03	Inf	-7.92	**<0.0001**	-0.21	0.03	Inf	-7.64	**<0.0001**
	RP *vs.* FF		-0.48	0.03	Inf	-18.33	**<0.0001**	-0.57	0.03	Inf	-22.28	**<0.0001**
	NF *vs.* FF		-0.26	0.02	Inf	-10.61	**<0.0001**	-0.36	0.02	Inf	-14.99	**<0.0001**
Spring	RP *vs.* NF		-0.07	0.02	Inf	-4.51	**<0.0001**	-0.12	0.02	Inf	-7.89	**<0.0001**
	RP *vs.* FF		-0.01	0.02	Inf	-0.32	0.9436	0.16	0.02	Inf	10.09	**<0.0001**
	NF *vs.* FF		0.06	0.02	Inf	4.19	**<0.0001**	0.28	0.02	Inf	17.92	**<0.0001**
Summer	RP *vs.* NF		-0.01	0.02	Inf	-0.37	0.9282	0.05	0.02	Inf	2.83	0.0129
	RP *vs.* FF		0.22	0.02	Inf	12.90	**<0.0001**	0.48	0.02	Inf	26.11	**<0.0001**
	NF *vs.* FF		0.23	0.02	Inf	13.26	**<0.0001**	0.44	0.02	Inf	23.39	**<0.0001**
LS0I												
Autumn	RP *vs.* NF		0.23	0.02	Inf	14.70	**<0.0001**	0.19	0.02	Inf	11.95	**<0.0001**
	RP *vs.* FF		0.07	0.02	Inf	4.79	**<0.0001**	0.19	0.02	Inf	11.92	**<0.0001**
	NF *vs.* FF		-0.16	0.02	Inf	-9.96	**<0.0001**	0.00	0.02	Inf	0.01	1.0000
Winter	RP *vs.* NF		0.04	0.01	Inf	3.42	0.0018	0.17	0.01	Inf	13.60	**<0.0001**
	RP *vs.* FF		0.26	0.01	Inf	20.42	**<0.0001**	0.18	0.01	Inf	14.49	**<0.0001**
	NF *vs.* FF		0.22	0.01	Inf	17.06	**<0.0001**	0.01	0.01	Inf	0.97	0.5978
Spring	RP *vs.* NF		0.00	0.01	Inf	-0.10	0.9942	0.04	0.01	Inf	2.49	0.0338
	RP *vs.* FF		-0.03	0.01	Inf	-2.18	0.0745	-0.12	0.01	Inf	-8.81	**<0.0001**
	NF *vs.* FF		-0.03	0.01	Inf	-2.09	0.0922	-0.16	0.01	Inf	-11.38	**<0.0001**
Summer	RP *vs.* NF		-0.09	0.01	Inf	-7.53	**<0.0001**	-0.09	0.01	Inf	-7.30	**<0.0001**
	RP *vs.* FF		-0.30	0.01	Inf	-25.56	**<0.0001**	-0.38	0.01	Inf	-32.89	**<0.0001**
	NF *vs.* FF		-0.21	0.01	Inf	-18.22	**<0.0001**	-0.29	0.01	Inf	-25.81	**<0.0001**
DS0I												
Autumn	RP *vs.* NF		-0.01	0.00	Inf	-3.15	**0.0046**	0.02	0.00	Inf	4.81	**<0.0001**
	RP *vs.* FF		-0.01	0.00	Inf	-1.64	0.2279	0.00	0.00	Inf	1.18	0.4628
	NF *vs.* FF		0.01	0.00	Inf	1.51	0.2850	-0.01	0.00	Inf	-3.63	**0.0008**
Winter	RP *vs.* NF		0.10	0.01	Inf	12.76	**<0.0001**	0.02	0.01	Inf	3.03	**0.0069**
	RP *vs.* FF		-0.03	0.01	Inf	-4.24	**<0.0001**	-0.10	0.01	Inf	-13.00	**<0.0001**
	NF *vs.* FF		-0.13	0.01	Inf	-16.98	**<0.0001**	-0.12	0.01	Inf	-16.01	**<0.0001**
Spring	RP *vs.* NF		-0.01	0.01	Inf	-1.83	0.1593	-0.01	0.01	Inf	-1.39	0.3461
	RP *vs.* FF		-0.05	0.01	Inf	-10.32	**<0.0001**	-0.12	0.01	Inf	-23.10	**<0.0001**
	NF *vs.* FF		-0.04	0.01	Inf	-8.49	**<0.0001**	-0.11	0.01	Inf	-21.72	**<0.0001**
Summer	RP *vs.* NF		0.00	0.00	Inf	0.50	0.8704	0.01	0.00	Inf	2.25	0.0626
	RP *vs.* FF		0.01	0.00	Inf	2.69	0.0195	0.01	0.00	Inf	1.84	0.1575
	NF *vs.* FF		0.01	0.00	Inf	2.19	0.0731	0.00	0.00	Inf	-0.42	0.9091

Table 3. Type II results of analyses of the microclimate: linear models of leaf wetness duration (LWD) and air temperature during the period of wetness (T) as a function of natural spatial variations in the climate ("Site" effect), discrepancies between the LWD model formalisms used to calculate LWD ("Models" effect), and the climatic periods ("Climatic change" effect), under future scenarios RCP 4.5 and 8.5. Significant effects are shown in bold. Details of the effects of different climatic periods are shown in Table 4.

| | Autumn | | | | | | Winter | | | | | | Spring | | | | | | Summer | | | | | |
| | RCP 4.5 | | | RCP 8.5 | | | RCP 4.5 | | | RCP 8.5 | | | RCP 4.5 | | | RCP 8.5 | | | RCP 4.5 | | | RCP 8.5 | | |
	F	df	Pr(>F)	F	df	Pr(>F)	F	df	Pr(>F)	F	df	Pr(>F)	F	df	Pr(>F)	F	df	Pr(>F)	F	df	Pr(>F)	F	df	Pr(>F)
LWD																								
LWD model	269.04	1	**<0.0001**	269.54	1	**<0.0001**	574.61	1	**<0.0001**	514.55	1	**<0.0001**	0.38	1	0.5356	0.86	1	0.3533	2.36	1	0.1254	2.83	1	0.0930
Climate change (CC)	14.85	2	**<0.0001**	35.57	2	**<0.0001**	0.54	2	0.5836	20.30	2	**<0.0001**	6.08	2	**0.0025**	46.82	2	**<0.0001**	30.56	2	**<0.0001**	94.06	2	**<0.0001**
Site	7.06	2	**0.0009**	12.17	2	**<0.0001**	14.52	2	**<0.0001**	5.49	2	**0.0044**	26.83	2	**<0.0001**	26.57	2	**<0.0001**	13.89	2	**<0.0001**	15.87	2	**<0.0001**
LWD model x CC	0.11	2	0.9003	1.59	2	0.2041	1.38	2	0.2514	3.20	2	0.0417	0.09	2	0.9140	0.10	2	0.9067	0.04	2	0.9652	0.17	2	0.8411
LWD model x Site	0.02	2	0.9813	0.06	2	0.9381	0.87	2	0.4181	0.85	2	0.4268	0.32	2	0.7264	0.67	2	0.5105	0.15	2	0.8602	0.10	2	0.9092
CC x Site	0.14	4	0.9668	0.68	4	0.6048	1.99	4	0.0947	0.35	4	0.8425	0.21	4	0.9312	0.42	4	0.7964	0.16	4	0.9577	0.55	4	0.7001
LWD model x CC x Site	0.01	4	0.9997	0.09	4	0.9844	0.09	4	0.9860	0.06	4	0.9935	0.04	4	0.9962	0.03	4	0.9982	0.00	4	1.0000	0.01	4	0.9998
T																								
LWD model	269.04	1	**<0.0001**	269.54	1	**<0.0001**	574.61	1	**<0.0001**	514.55	1	**<0.0001**	0.38	1	0.5356	0.86	1	0.3533	2.36	1	0.1254	2.83	1	0.0930
Climate change (CC)	14.85	2	**<0.0001**	35.57	2	**<0.0001**	0.54	2	0.5836	20.30	2	**<0.0001**	6.08	2	**0.0025**	46.82	2	**<0.0001**	30.56	2	**<0.0001**	94.06	2	**<0.0001**
Site	7.06	2	**0.0009**	12.17	2	**<0.0001**	14.52	2	**<0.0001**	5.49	2	**0.0044**	26.83	2	**<0.0001**	26.57	2	**<0.0001**	13.89	2	**<0.0001**	15.87	2	**<0.0001**
LWD model x CC	0.11	2	0.9003	1.59	2	0.2041	1.38	2	0.2514	3.20	2	0.0417	0.09	2	0.9140	0.10	2	0.9067	0.04	2	0.9652	0.17	2	0.8411
LWD model x Site	0.02	2	0.9813	0.06	2	0.9381	0.87	2	0.4181	0.85	2	0.4268	0.32	2	0.7264	0.67	2	0.5105	0.15	2	0.8602	0.10	2	0.9092
CC x Site	0.14	4	0.9668	0.68	4	0.6048	1.99	4	0.0947	0.35	4	0.8425	0.21	4	0.9312	0.42	4	0.7964	0.16	4	0.9577	0.55	4	0.7001
LWD model x CC x Site	0.01	4	0.9997	0.09	4	0.9844	0.09	4	0.9860	0.06	4	0.9935	0.04	4	0.9962	0.03	4	0.9982	0.00	4	1.0000	0.01	4	0.9998

Table 4: Pairwise comparison of the seasonal effects of climatic periods (recent past period "RP": 1976-2005; near future period "NF": 2021-2050 and far future period "FF": 2070-2099) on leaf wetness duration and air temperature during the period of wetness under scenarios RCP 4.5 and 8.5.

	Climatic periods	Leaf wetness duration (LWD)				Temperature during leaf wetness duration (T)			
		RCP 4.5		RCP 8.5		RCP 4.5		RCP 8.5	
		diff	*P adj*	diff	*P adj*	diff	*P adj*	diff	*P adj*
Autumn	RP *vs.* NF	-0.25	0.2262	0.15	0.5902	-1.48	**<0.0001**	-1.40	**<0.0001**
	RP *vs.* FF	0.55	**0.0008**	1.16	**<0.0001**	-1.66	**<0.0001**	-3.33	**<0.0001**
	NF *vs.* FF	0.79	**<0.0001**	1.01	**<0.0001**	-0.18	0.3803	-1.93	**<0.0001**
Winter	RP *vs.* NF	-0.03	0.9597	0.01	0.9941	-1.00	**<0.0001**	-0.92	**<0.0001**
	RP *vs.* FF	0.08	0.7452	0.64	**<0.0001**	-2.14	**<0.0001**	-2.80	**<0.0001**
	NF *vs.* FF	0.10	0.5746	0.63	**<0.0001**	-1.13	**<0.0001**	-1.88	**<0.0001**
Spring	RP *vs.* NF	0.05	0.9718	-0.18	0.6526	-0.75	**<0.0001**	-0.91	**<0.0001**
	RP *vs.* FF	0.65	**0.0053**	1.57	**<0.0001**	-1.53	**<0.0001**	-2.50	**<0.0001**
	NF *vs.* FF	0.61	0.0109	1.75	**<0.0001**	-0.78	**<0.0001**	-1.59	**<0.0001**
Summer	RP *vs.* NF	0.35	0.1939	0.62	**0.0036**	-0.99	**<0.0001**	-1.15	**<0.0001**
	RP *vs.* FF	1.50	**<0.0001**	2.51	**<0.0001**	-1.99	**<0.0001**	-3.56	**<0.0001**
	NF *vs.* FF	1.15	**<0.0001**	1.89	**<0.0001**	-1.01	**<0.0001**	-2.41	**<0.0001**

Figure 1: Description of the protocol for the *in silico* study. The surface responses of the relative infection efficiency of leaf rust of wheat to leaf wetness duration and temperature during wetness periods are shown for the Pope model (de Vallavieille-Pope et al., 1995) (a), and the ClimInfeR model (Launay et al., 2014) (b). The wetness required to reach 5% infection efficiency for leaf rust of wheat at different temperatures is shown for the Magarey model (Magarey, 2005) (c).

Physical model
PLATA

RCP 4.5 & 8.5 scenarios of future CO_2 emissions

Global climate model, ALADIN

Quantile-quantile downscaling method

Estrées-Mons 49.5°

Versailles 48.8°

Bordeaux 44.8°

Future daily climatic data for three locations in France

Hourly

assessment

Hourly rainfall (mm) and relative humidity (%)

Statistical model
MEDHI

Leaf Wetness Duration (hours) (assessed by PLATA & assessed by MEDHI)

Hourly Temperatures (°C)

Pope model (a)

ClimInfeR model (b)

Magarey model (c)

Temperature (°C)

Leaf wetness duration (hour)

Temperature (°C)

Leaf wetness duration (hour)

Temperature (°C)

Daily infection efficiency ([0-1]) assessed by the Pope model & assessed by the ClimInfeR model

Infectious day (Yes or No)

Climatic indicators of infection risk
- Number of infectious days throughout a period (NID & NID5)
- Global risk of infection throughout a period (GIR) from the number of infectious days and the mean infection efficiency during these days
- Length and date of the longest sequence without infection throughout a period (LS0I & DS0I)

Figure 2: Number of days with an infection efficiency higher than 5% throughout a 30-day sliding period (NID5) (a) and global risk of infection throughout a 30-day sliding period (GIR) (b), simulated by the six combinations of models coupling the two wetness duration models Medhi and Plata with the three infection models Pope, ClimInfeR and Magarey. Moving values for NID5 (a) and GIR (b) are shown from 1950 to 2100 (x-axis), from January 1st to December 31 (y-axis), and shown from low values (blue) to high values (red). Results are shown for the climatic situation at the Versailles site under the RCP 8.5 scenario.
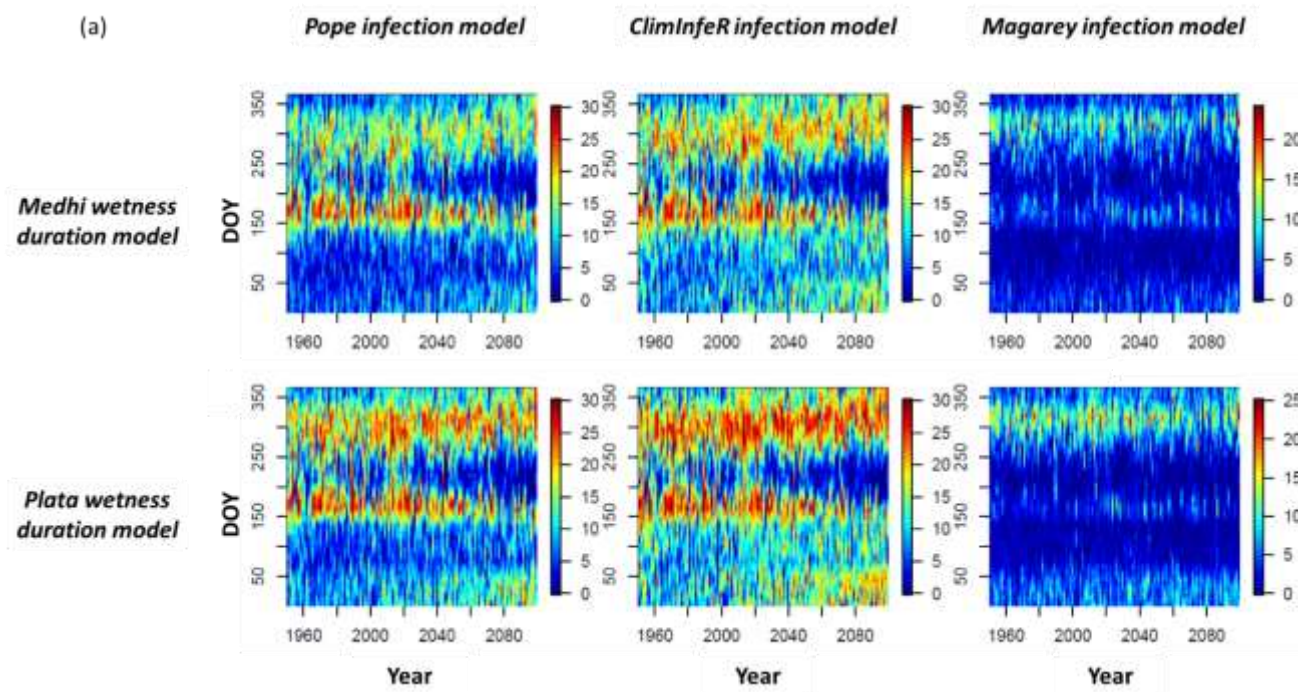
(b)
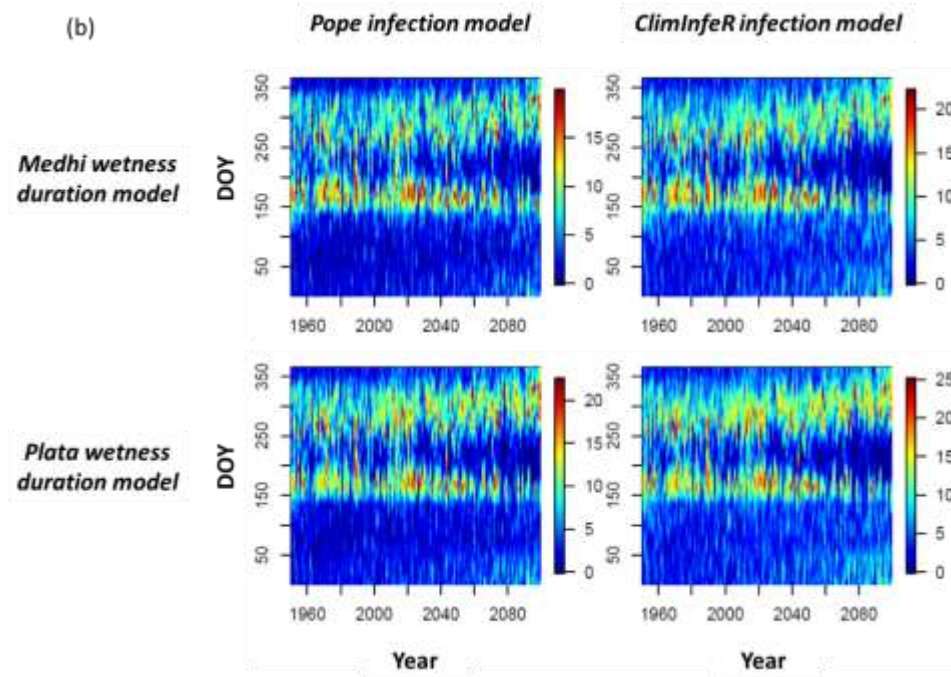
Figure 3: Number of days with infection efficiency higher than 5% NID5 (a, c, e and g) and a global risk of infection GIR (b, d, f, h) over the four seasons (autumn, winter, spring and summer) in the near and far future compared to the recent past, at Versailles under scenario RCP 8.5. NID5 values were calculated by the six modeling combinations coupling the two wetness duration models Medhi and Plata with the three infection models Pope, ClimInfeR and Magarey, while GIR values were calculated by the four modeling combinations coupling the Medhi and Plata models with Pope and ClimInfeR. Values are sums (NID5) and means (GIR) ± S.E.M (crosses).
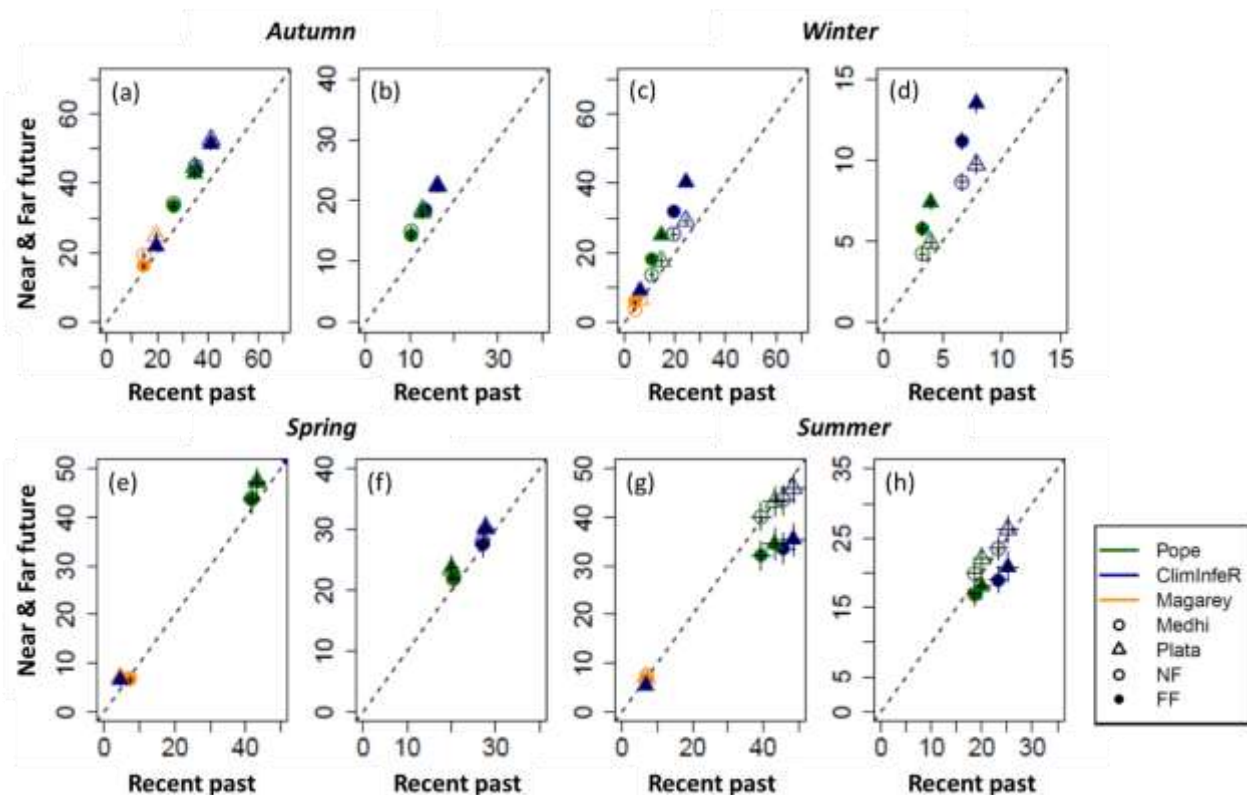
Figure 4: Maximum length (number of days) of LS0I periods without infection over the four seasons (autumn (a), winter (b), spring (c) and summer (d)) in the near and far future compared to the recent past at Versailles under scenario RCP 8.5. LS0I values were calculated by the six modeling combinations coupling the two wetness duration models Medhi and Plata with the three infection models Pope, ClimInfeR and Magarey. Values are sums ± S.E.M (crosses).

Autumn

(a)

Near & Far future

Recent past

Winter

(b)

Recent past

Spring

(c)

Near & Far future

Recent past

Summer

(d)

Recent past

Pope
ClimInfeR
Magarey
○ Medhi
△ Plata
○ NF
● FF
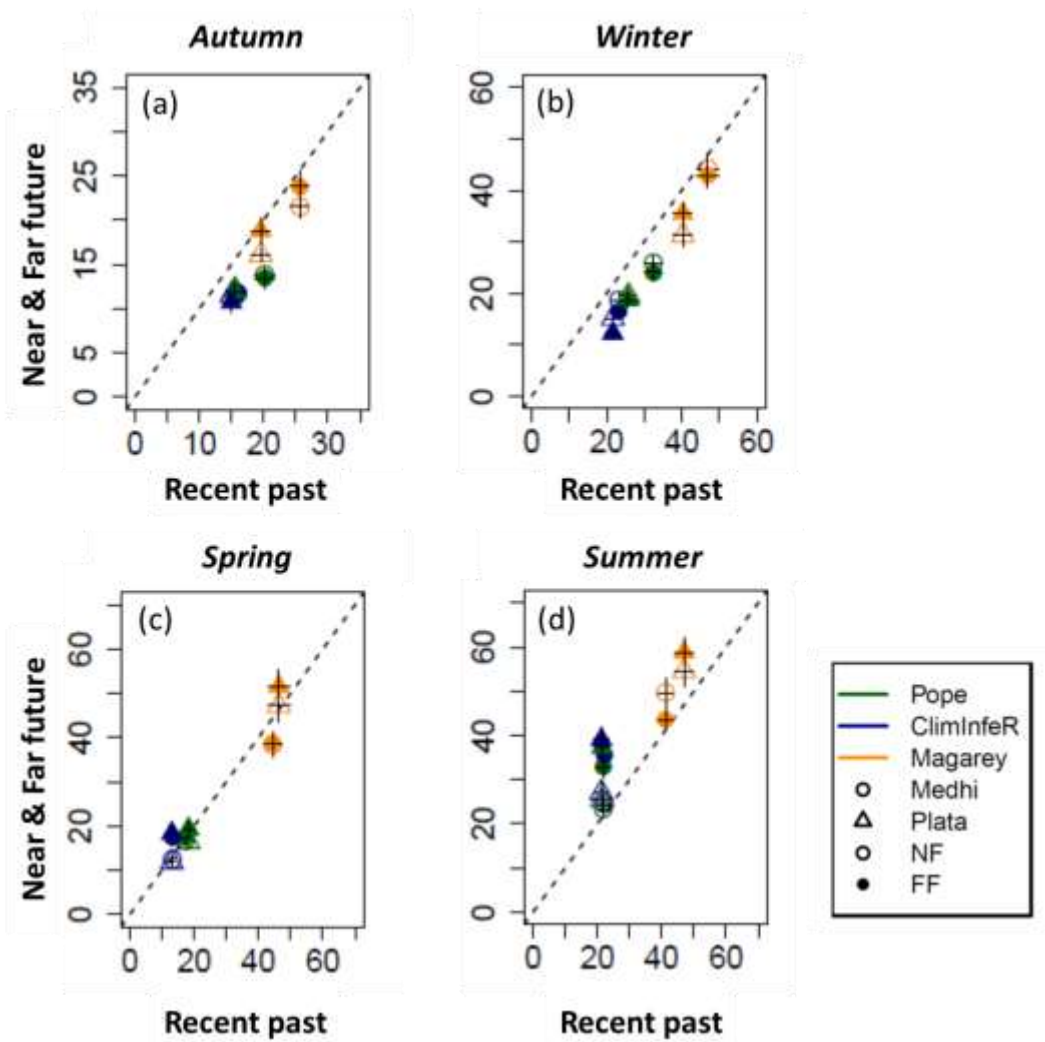
Figure 5: Compared evolutions of the relative global risk of infection GIR and maximum length of periods without infection LS0I, with relative leaf wetness durations LWD and temperature during wetness periods over the four seasons (autumn, winter, spring and summer), in the near and far future (NF and FF, respectively) at the Bordeaux, Mons and Versailles sites and under RCP scenarios 4.5 and 8.5.
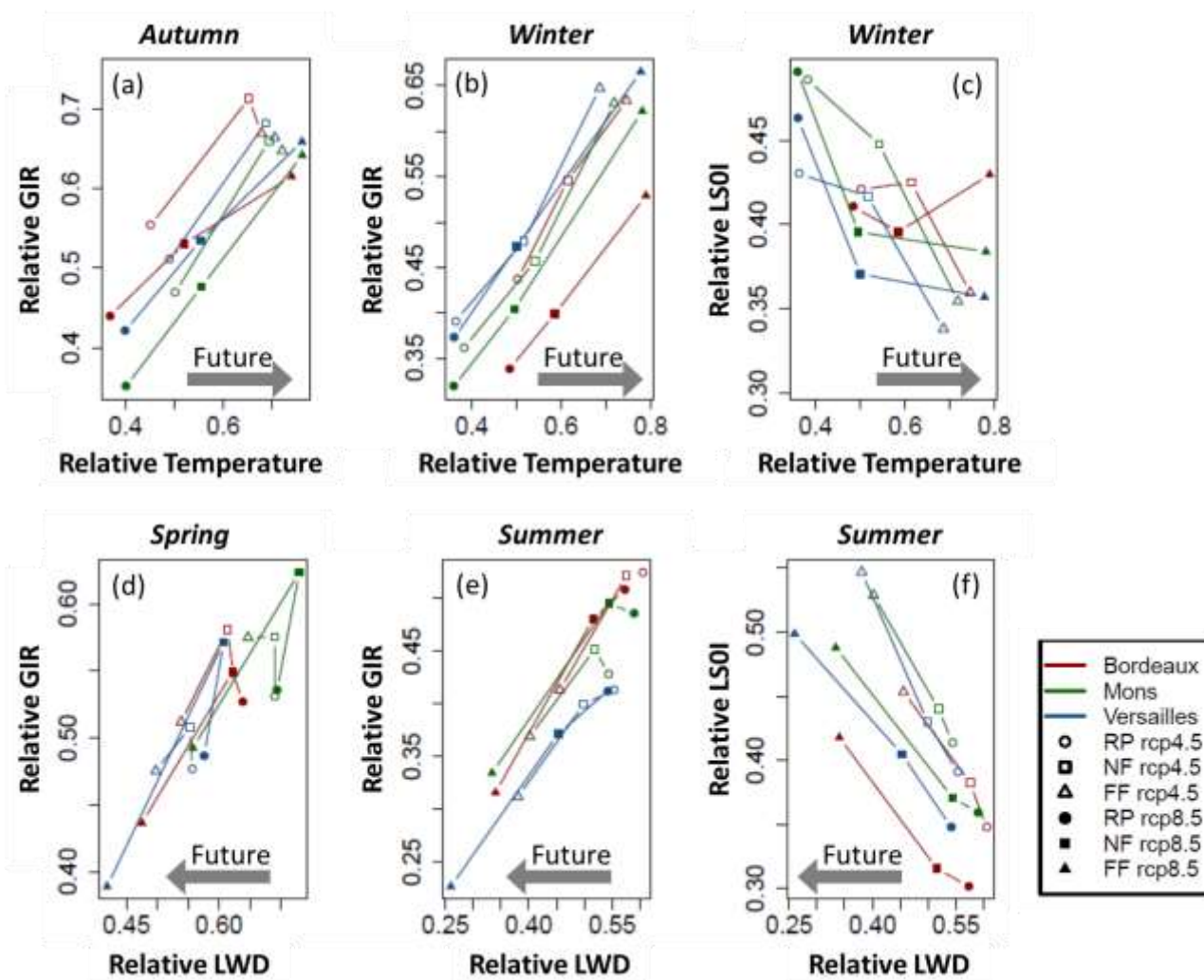
Figure 6: Surface responses of the relative infection efficiency of leaf rust of wheat as simulated by the Pope model (top left) and ClimInfeR model (bottom left), and the same surface responses when pairs of (temperature, leaf wetness duration) values were subtracted, where the Magarey model simulated an infection efficiency < 5% (right).
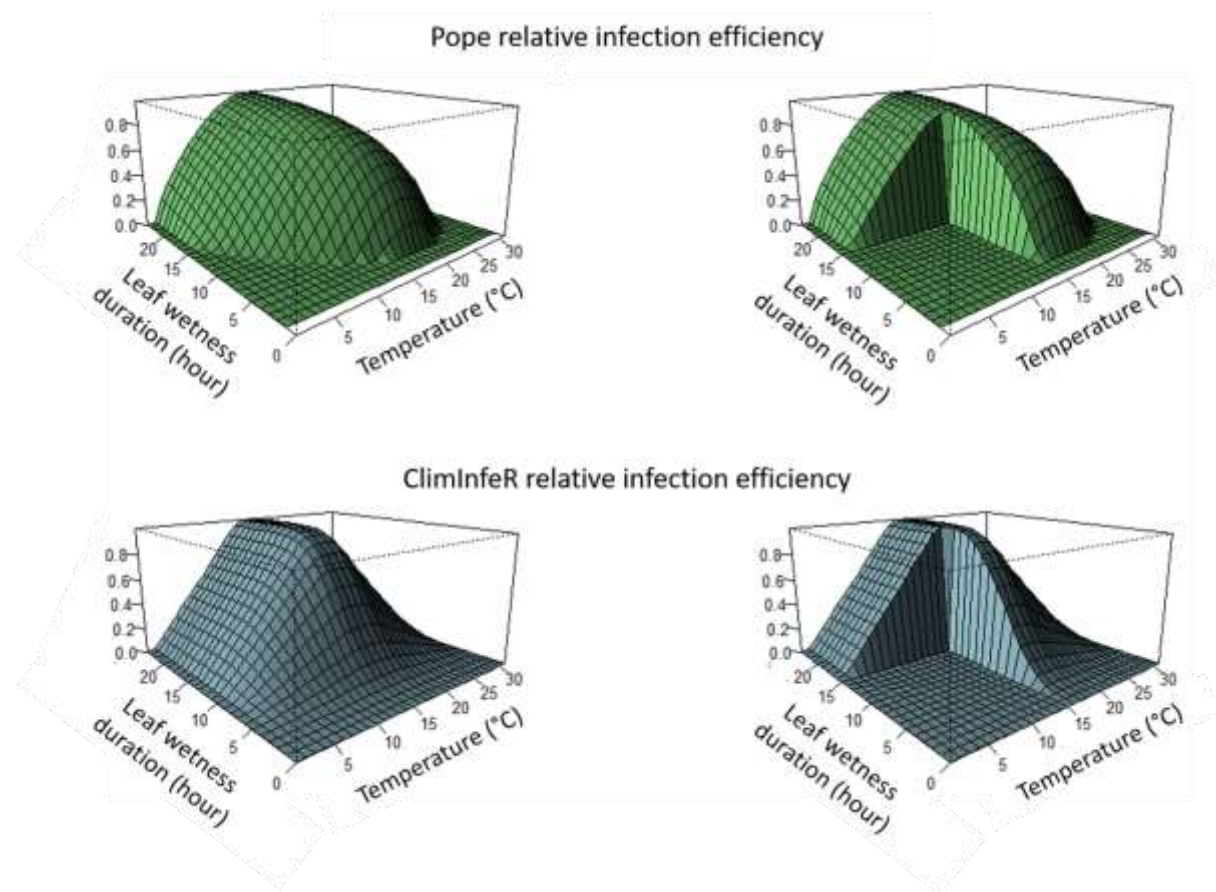
Appendix A. Mean seasonal values of the NID5, GIR, LS0I, DS0I, LWD and T climatic indicators.

Values are given for RCP scenarios 4.5 and 8.5 at the Bordeaux, Estrées-Mons and Versailles sites, for climatic periods in the recent past "RP" (1976-2005), near future "NF" (2021-2050) and far future "FF" (2070-2099) and for all combinations of models.

a) Mean seasonal NID5 values: cumulated number of days with at least 5% of infection efficiency

Season	Combination of models	RCP 4.5 scenario									RCP 8.5 scenario								
		Bordeaux			Estrées-Mons			Versailles			Bordeaux			Estrées-Mons			Versailles		
		RP	NF	FF	RP	NF	FF	RP	NF	FF	RP	NF	FF	RP	NF	FF	RP	NF	FF
Autumn	Medhi Pope	37	44	41	26	34	33	31	37	36	36	42	44	26	33	41	31	34	39
	Medhi ClimInfeR	47	53	50	35	45	44	39	47	46	47	52	52	35	44	51	39	46	49
	Medhi Magarey	18	21	17	15	19	16	17	21	18	18	17	16	15	17	17	17	18	16
	Plata Pope	48	55	52	35	45	43	40	47	47	48	53	54	35	43	50	41	47	49
	Plata ClimInfeR	55	62	60	41	53	51	47	55	56	55	61	61	42	52	58	48	54	58
	Plata Magarey	25	29	25	20	25	22	23	28	25	27	27	23	19	22	22	24	26	23
	****	**38**	**44**	**41**	**29**	**37**	**35**	**33**	**39**	**38**	**39**	**42**	**42**	**29**	**35**	**40**	**33**	**38**	**39**
Winter	Medhi Pope	20	25	28	11	14	18	13	16	21	20	24	29	10	14	19	13	17	22
	Medhi ClimInfeR	34	40	43	20	25	32	23	26	33	34	39	42	20	26	34	23	28	35
	Medhi Magarey	7	7	7	4	4	6	6	5	6	7	6	7	4	4	5	5	6	6
	Plata Pope	31	37	41	15	18	25	18	21	29	31	36	43	15	19	27	20	24	30
	Plata ClimInfeR	44	49	55	24	29	40	28	32	41	44	50	55	24	32	42	29	37	45
	Plata Magarey	12	13	13	6	7	9	9	9	12	13	12	14	7	7	9	9	11	11
	****	**24**	**28**	**31**	**13**	**16**	**22**	**16**	**18**	**24**	**25**	**28**	**32**	**13**	**17**	**23**	**16**	**20**	**25**
Spring	Medhi Pope	46	47	42	42	44	44	36	38	36	46	46	39	42	47	40	36	40	31
	Medhi ClimInfeR	51	50	45	52	53	52	43	43	40	51	49	39	52	57	47	43	45	34
	Medhi Magarey	7	9	8	7	7	7	6	7	6	7	8	9	6	8	8	6	8	6
	Plata Pope	49	50	46	43	47	47	36	39	37	49	50	42	43	50	42	37	42	30
	Plata ClimInfeR	55	54	49	56	58	56	44	45	42	55	54	42	56	62	49	45	48	34
	Plata Magarey	6	8	8	5	7	7	4	5	5	7	8	9	4	7	7	5	7	5
	****	**36**	**36**	**33**	**34**	**36**	**35**	**28**	**30**	**28**	**36**	**36**	**30**	**34**	**38**	**32**	**28**	**32**	**23**
Summer	Medhi Pope	39	37	31	39	40	32	33	32	24	39	37	24	40	38	26	33	29	18
	Medhi ClimInfeR	40	37	29	46	44	34	36	33	25	39	35	22	45	42	25	35	30	17
	Medhi Magarey	10	10	10	7	7	7	8	8	7	10	10	12	7	7	6	8	7	6
	Plata Pope	42	41	34	43	43	35	36	35	26	43	41	27	43	42	28	36	32	19
	Plata ClimInfeR	42	41	32	48	46	36	39	36	27	43	39	24	49	46	28	39	33	18
	Plata Magarey	10	12	11	7	7	5	8	7	6	11	11	12	7	7	5	9	7	6
	****	**31**	**30**	**24**	**32**	**31**	**25**	**27**	**25**	**19**	**31**	**29**	**20**	**32**	**30**	**20**	**27**	**23**	**14**

b) Mean seasonal GIR values: equivalent to the cumulated number of days of full infection (100% infection efficiency)

Season	Combination of models	RCP 4.5 scenario									RCP 8.5 scenario								
		Bordeaux			Estrées-Mons			Versailles			Bordeaux			Estrées-Mons			Versailles		
		RP	NF	FF	RP	NF	FF	RP	NF	FF	RP	NF	FF	RP	NF	FF	RP	NF	FF
Autumn	Medhi Pope	17	22	20	10	15	14	13	17	16	16	20	24	10	14	19	13	16	20
	Medhi ClimInfeR	21	26	25	13	18	18	16	21	20	21	25	29	13	18	25	15	20	25
	Plata Pope	22	28	26	13	19	18	16	22	21	22	27	30	13	18	24	16	21	25
	Plata ClimInfeR	26	33	31	16	22	22	19	25	25	26	31	36	16	22	29	19	25	30
	mean	**21**	**27**	**26**	**13**	**19**	**18**	**16**	**21**	**21**	**21**	**26**	**30**	**13**	**18**	**24**	**16**	**20**	**25**
Winter	Medhi Pope	7	9	11	3	4	6	4	5	7	7	9	12	3	4	7	4	5	8
	Medhi ClimInfeR	13	16	18	7	9	11	8	10	12	13	15	19	7	9	12	8	10	14
	Plata Pope	10	13	16	4	5	7	5	7	10	11	13	18	4	5	8	6	7	11
	Plata ClimInfeR	16	20	23	8	10	14	9	11	15	17	20	25	8	10	15	10	12	17
	mean	**12**	**15**	**17**	**5**	**7**	**9**	**7**	**8**	**11**	**12**	**14**	**18**	**5**	**7**	**11**	**7**	**9**	**12**
Spring	Medhi Pope	23	25	22	21	22	22	18	19	18	23	24	21	21	24	19	18	21	15
	Medhi ClimInfeR	27	29	25	27	28	27	22	23	21	28	28	22	27	30	23	22	25	17
	Plata Pope	25	27	24	20	23	24	17	19	18	26	28	23	20	25	21	17	21	14
	Plata ClimInfeR	30	31	27	28	30	30	22	23	22	31	32	24	28	33	25	22	26	17
	mean	**26**	**28**	**24**	**24**	**26**	**26**	**20**	**21**	**20**	**27**	**28**	**22**	**24**	**28**	**22**	**20**	**23**	**16**
Summer	Medhi Pope	22	21	17	19	20	17	17	17	13	22	21	14	19	19	14	17	15	10
	Medhi ClimInfeR	23	22	17	23	24	19	20	19	14	23	21	13	23	23	14	20	17	10
	Plata Pope	24	25	20	20	22	18	18	18	14	25	24	17	20	21	15	19	17	11
	Plata ClimInfeR	26	26	20	25	26	21	22	21	16	26	25	15	25	26	17	22	20	11
	mean	**24**	**24**	**19**	**22**	**23**	**19**	**19**	**19**	**14**	**24**	**23**	**15**	**22**	**22**	**15**	**19**	**18**	**11**

c) Mean seasonal LS0I values: number of days of the longest sequence during which infection efficiency is lower than 5%.

Season	Combination of models	RCP 4.5 scenario									RCP 8.5 scenario								
		Bordeaux			Estrées-Mons			Versailles			Bordeaux			Estrées-Mons			Versailles		
		RP	NF	FF	RP	NF	FF	RP	NF	FF	RP	NF	FF	RP	NF	FF	RP	NF	FF
Autumn	Medhi Pope	15	12	15	21	16	18	19	15	15	15	14	13	21	17	14	20	14	13
	Medhi ClimInfeR	12	10	13	18	14	16	16	12	14	12	11	11	18	14	13	16	12	12
	Medhi Magarey	23	20	25	28	20	26	27	22	24	23	24	26	27	22	23	26	22	24
	Plata Pope	12	10	14	18	14	15	16	12	13	12	11	12	19	14	13	16	12	12
	Plata ClimInfeR	11	9	11	16	13	14	15	11	12	11	10	10	17	13	12	15	12	11
	Plata Magarey	16	15	20	22	17	20	21	17	18	16	18	20	23	18	19	20	16	19
	—	**15**	**13**	**16**	**21**	**16**	**18**	**19**	**15**	**16**	**15**	**14**	**15**	**21**	**16**	**16**	**19**	**14**	**15**
Winter	Medhi Pope	23	22	18	34	31	23	31	28	23	23	21	21	34	26	27	32	26	24
	Medhi ClimInfeR	17	17	13	27	24	17	22	22	16	16	14	15	28	20	17	23	19	16
	Medhi Magarey	44	44	43	50	52	45	43	47	44	41	44	49	47	49	51	47	44	43
	Plata Pope	16	16	14	31	27	20	27	25	18	16	15	17	29	22	21	26	20	19
	Plata ClimInfeR	12	12	8	25	21	14	21	19	13	12	11	11	26	17	13	22	15	12
	Plata Magarey	32	35	30	43	44	38	39	38	33	29	32	37	41	36	39	40	31	36
	—	**24**	**24**	**21**	**35**	**33**	**26**	**30**	**30**	**25**	**23**	**23**	**25**	**34**	**28**	**28**	**32**	**26**	**25**
Spring	Medhi Pope	13	15	14	18	17	17	18	17	17	12	14	15	17	16	16	17	17	17
	Medhi ClimInfeR	9	12	14	13	12	12	14	14	17	9	12	15	13	11	15	13	13	17
	Medhi Magarey	47	44	45	45	43	44	46	45	43	49	40	41	42	41	42	44	38	39
	Plata Pope	11	13	13	18	15	16	18	16	18	12	14	14	17	13	16	18	16	19
	Plata ClimInfeR	9	11	11	12	10	10	13	13	15	9	11	15	12	9	15	13	12	18
	Plata Magarey	46	50	49	50	51	52	53	49	48	47	44	47	51	49	57	46	47	52
	—	**22**	**24**	**24**	**26**	**24**	**25**	**27**	**26**	**26**	**23**	**23**	**25**	**25**	**23**	**27**	**25**	**24**	**27**
Summer	Medhi Pope	17	20	24	18	18	25	22	24	30	17	19	30	18	18	28	22	23	33
	Medhi ClimInfeR	17	21	26	17	19	25	21	25	32	18	21	34	17	18	28	22	24	36
	Medhi Magarey	40	37	42	46	45	43	43	42	51	42	40	41	47	43	50	41	50	43
	Plata Pope	16	19	24	18	19	26	22	23	35	16	17	29	17	19	27	21	25	37
	Plata ClimInfeR	16	21	26	17	19	26	21	24	35	16	19	32	16	19	28	21	27	39
	Plata Magarey	45	42	45	50	55	57	47	55	59	44	42	40	52	53	59	47	55	59
	—	**25**	**27**	**31**	**28**	**29**	**34**	**29**	**32**	**40**	**25**	**26**	**35**	**28**	**28**	**36**	**29**	**34**	**41**

d) Mean seasonal DS0I values: median date of the longest sequence during which infection efficiency is lower than 5% (DOY).

Season	Combination of models	RCP 4.5 scenario									RCP 8.5 scenario								
		Bordeaux			Estrées-Mons			Versailles			Bordeaux			Estrées-Mons			Versailles		
		RP	NF	FF	RP	NF	FF	RP	NF	FF	RP	NF	FF	RP	NF	FF	RP	NF	FF
Autumn	Medhi Pope	343	348	344	347	345	344	347	338	339	347	345	329	348	345	343	342	344	332
	Medhi ClimInfeR	280	263	272	238	247	265	243	287	248	271	239	303	228	240	241	243	216	251
	Medhi Magarey	340	332	336	343	337	336	346	341	334	343	341	322	348	345	333	350	341	329
	Plata Pope	348	346	351	346	343	342	347	338	347	351	347	339	348	346	348	348	349	338
	Plata ClimInfeR	250	252	285	250	259	263	250	298	237	260	262	317	237	240	243	252	239	233
	Plata Magarey	338	339	345	347	334	338	339	338	335	335	340	329	342	332	336	339	339	327
	336	**316**	**313**	**322**	**312**	**311**	**315**	**312**	**323**	**307**	**318**	**312**	**323**	**308**	**308**	**307**	**312**	**305**	**302**
Winter	Medhi Pope	65	56	63	62	52	65	67	53	68	60	61	65	58	66	64	65	63	63
	Medhi ClimInfeR	57	53	64	62	50	59	63	52	65	58	54	70	53	52	61	62	53	64
	Medhi Magarey	76	70	72	64	58	71	69	64	73	71	71	75	63	64	71	67	68	71
	Plata Pope	68	58	66	62	58	62	66	62	70	67	65	78	63	66	72	65	60	72
	Plata ClimInfeR	59	51	63	55	53	57	56	57	59	55	54	73	55	46	58	59	54	66
	Plata Magarey	80	74	78	70	68	78	72	75	77	80	78	80	67	73	76	72	70	78
		67	**60**	**68**	**62**	**57**	**65**	**66**	**61**	**69**	**65**	**64**	**73**	**60**	**61**	**67**	**65**	**61**	**69**
Spring	Medhi Pope	126	133	139	128	128	136	128	130	145	122	131	149	127	132	154	131	128	154
	Medhi ClimInfeR	137	137	146	131	132	146	129	145	152	138	139	157	128	137	163	134	138	161
	Medhi Magarey	143	134	135	134	139	129	134	133	134	140	131	133	135	130	135	136	137	140
	Plata Pope	122	134	139	129	127	136	132	128	145	124	132	151	130	135	151	130	124	157
	Plata ClimInfeR	136	140	144	132	135	141	133	137	153	137	136	151	131	136	161	135	139	166
	Plata Magarey	136	134	134	140	136	135	145	136	138	141	137	140	137	136	135	138	134	140
		133	**135**	**140**	**132**	**133**	**137**	**133**	**135**	**144**	**134**	**134**	**147**	**131**	**134**	**150**	**134**	**133**	**153**
Summer	Medhi Pope	233	234	230	241	236	230	233	237	230	232	234	234	241	233	230	231	230	227
	Medhi ClimInfeR	233	231	227	236	234	229	230	230	227	232	233	234	239	228	231	231	229	230
	Medhi Magarey	228	234	234	237	237	231	235	232	234	228	234	231	238	237	239	234	231	237
	Plata Pope	231	229	230	237	233	231	233	232	227	231	233	234	239	227	228	234	228	228
	Plata ClimInfeR	231	229	231	233	232	231	228	229	227	231	229	234	235	230	228	225	227	228
	Plata Magarey	227	229	235	234	231	232	231	230	231	229	231	230	234	229	230	230	231	230
		231	**231**	**231**	**236**	**234**	**230**	**231**	**232**	**229**	**230**	**232**	**233**	**238**	**231**	**231**	**231**	**229**	**230**

e) Mean seasonal LWD values: average leaf wetness duration (hours)

Season	Combination of models	RCP 4.5 scenario									RCP 8.5 scenario								
		Bordeaux			Estrées-Mons			Versailles			Bordeaux			Estrées-Mons			Versailles		
		RP	NF	FF	RP	NF	FF	RP	NF	FF	RP	NF	FF	RP	NF	FF	RP	NF	FF
Autumn	Medhi	9.7	10.1	9.2	10.3	10.6	9.9	10.1	10.4	9.6	9.7	9.5	8.7	10.3	10.3	9.6	10.1	10.0	9.1
	Plata	11.8	12.1	11.2	12.3	12.5	11.8	12.2	12.3	11.6	12.0	11.7	10.3	12.3	12.3	11.4	12.4	12.0	10.9
	****	**10.7**	**11.1**	**10.2**	**11.3**	**11.5**	**10.8**	**11.2**	**11.4**	**10.6**	**10.8**	**10.6**	**9.5**	**11.3**	**11.3**	**10.5**	**11.3**	**11.0**	**10.0**
Winter	Medhi	7.2	7.5	7.3	7.2	7.1	7.3	6.8	6.8	7.0	7.2	7.2	6.8	7.2	7.1	6.8	6.9	7.0	6.5
	Plata	9.5	9.9	9.2	9.3	9.0	9.1	9.0	8.8	8.8	9.7	9.6	8.8	9.4	9.2	8.5	9.2	9.3	8.2
	****	**8.4**	**8.7**	**8.2**	**8.3**	**8.1**	**8.2**	**7.9**	**7.8**	**7.9**	**8.5**	**8.4**	**7.8**	**8.3**	**8.1**	**7.6**	**8.0**	**8.2**	**7.4**
Spring	Medhi	6.5	6.4	5.6	7.2	7.1	6.6	5.9	5.8	5.1	6.5	6.3	4.9	7.2	7.4	5.7	5.9	6.1	4.3
	Plata	6.7	6.6	5.8	7.2	7.4	6.9	5.7	5.7	5.2	6.9	6.8	5.1	7.2	7.7	5.9	5.8	6.2	4.2
	****	**6.6**	**6.5**	**5.7**	**7.2**	**7.2**	**6.8**	**5.8**	**5.7**	**5.1**	**6.7**	**6.5**	**5.0**	**7.2**	**7.6**	**5.8**	**5.8**	**6.1**	**4.2**
Summer	Medhi	5.2	4.9	3.9	6.0	5.7	4.4	5.0	4.5	3.5	5.2	4.7	3.1	6.0	5.5	3.4	5.0	4.2	2.4
	Plata	5.5	5.3	4.2	6.2	5.9	4.6	5.2	4.7	3.6	5.6	5.1	3.3	6.2	5.8	3.5	5.3	4.5	2.5
	****	**5.4**	**5.1**	**4.0**	**6.1**	**5.8**	**4.5**	**5.1**	**4.6**	**3.5**	**5.4**	**4.9**	**3.2**	**6.1**	**5.6**	**3.5**	**5.2**	**4.3**	**2.5**

f) Mean seasonal T values: average air temperature during wetness periods (°C).

Season	Combination of models	RCP 4.5 scenario									RCP 8.5 scenario								
		Bordeaux			Estrées-Mons			Versailles			Bordeaux			Estrées-Mons			Versailles		
		RP	NF	FF	RP	NF	FF	RP	NF	FF	RP	NF	FF	RP	NF	FF	RP	NF	FF
Autumn	Medhi	6.4	7.9	8.1	4.2	5.7	5.8	4.9	6.4	6.5	6.3	7.8	9.7	4.1	5.7	7.6	4.9	6.3	8.2
	Plata	6.6	8.0	8.3	4.2	5.6	5.9	5.0	6.4	6.6	6.6	7.9	9.9	4.2	5.6	7.5	5.0	6.3	8.2
	****	**6.5**	**8.0**	**8.2**	**4.2**	**5.6**	**5.9**	**4.9**	**6.4**	**6.5**	**6.5**	**7.9**	**9.8**	**4.2**	**5.6**	**7.6**	**4.9**	**6.3**	**8.2**
Winter	Medhi	5.7	6.6	7.6	3.2	4.3	5.5	3.9	5.0	6.0	5.6	6.5	8.3	3.2	4.2	6.2	3.9	4.9	6.7
	Plata	5.9	6.8	7.9	3.2	4.2	5.5	3.9	4.8	6.1	5.9	6.8	8.5	3.2	4.2	6.2	3.9	4.9	6.8
	****	**5.8**	**6.7**	**7.7**	**3.2**	**4.3**	**5.5**	**3.9**	**4.9**	**6.1**	**5.8**	**6.7**	**8.4**	**3.2**	**4.2**	**6.2**	**3.9**	**4.9**	**6.7**
Spring	Medhi	13.0	13.8	14.5	10.8	11.5	12.4	11.9	12.7	13.4	12.9	13.8	15.9	10.8	11.7	13.3	11.8	12.7	14.4
	Plata	12.7	13.5	14.2	10.5	11.3	12.1	11.4	12.0	12.8	12.8	13.6	15.4	10.5	11.5	12.7	11.4	12.3	13.5
	****	**12.8**	**13.6**	**14.4**	**10.6**	**11.4**	**12.3**	**11.6**	**12.4**	**13.1**	**12.9**	**13.7**	**15.6**	**10.7**	**11.6**	**13.0**	**11.6**	**12.5**	**13.9**
Summer	Medhi	14.9	15.8	17.0	12.3	13.3	14.4	13.2	14.2	15.4	14.9	16.1	18.8	12.2	13.4	16.0	13.2	14.4	17.2
	Plata	14.7	15.5	16.4	11.9	12.9	13.7	12.7	13.7	14.6	14.8	15.8	18.1	11.9	13.0	15.0	12.7	13.7	15.9
	****	**14.8**	**15.7**	**16.7**	**12.1**	**13.1**	**14.1**	**12.9**	**14.0**	**15.0**	**14.8**	**16.0**	**18.5**	**12.1**	**13.2**	**15.5**	**13.0**	**14.1**	**16.5**

1 **Appendix B. Representation of the fourteen trials performed during the 1990-2015 period**
2 **and three French climate patterns.**
3
4 Distribution of cumulated rainfall (mm) and temperatures (°C) from January 1st to March 31 (a)
5 and from April 1st to June 30 (b) in pure oceanic (OCEA), Mediterranean (MEDI) and
6 southwestern (SOWE) climatic conditions in France from 1990 to 2015. The fourteen trials used
7 for the calibration and evaluation dataset are identified by numbers (see Table 2).

8
9